

Fluid flow and Al transport during quartz-kyanite vein formation, Unst, Shetland Islands, Scotland

C. E. BUCHOLZ AND J. J. AGUE

Department of Geology & Geophysics, Yale University, New Haven, PO Box 208109, CT 06520-8109, USA
(jay.ague@yale.edu)

ABSTRACT Quartz-kyanite veins, adjacent alteration selvages and surrounding ‘precursor’ wall rocks in the Dalradian Saxa Vord Pelite of Unst in the Shetland Islands (Scotland) were investigated to constrain the geochemical alteration and mobility of Al associated with channelized metamorphic fluid infiltration during the Caledonian Orogeny. Thirty-eight samples of veins, selvages and precursors were collected, examined using the petrographic microscope and electron microprobe, and geochemically analysed. With increasing grade, typical precursor mineral assemblages include, but are not limited to, chlorite + chloritoid, chlorite + chloritoid + kyanite, chlorite + chloritoid + staurolite and garnet + staurolite + kyanite + chloritoid. These assemblages coexist with quartz, white mica (muscovite, paragonite, margarite), and Fe-Ti oxides. The mineral assemblage of the selvages does not change noticeably with metamorphic grade, and consists of chloritoid, kyanite, chlorite, quartz, white mica and Fe-Ti oxides. Pseudosections for selvage and precursor bulk compositions indicate that the observed mineral assemblages were stable at regional metamorphic conditions of 550–600 °C and 0.8–1.1 GPa. A mass balance analysis was performed to assess the nature and magnitude of geochemical alteration that produced the selvages adjacent to the veins. On average, selvages lost about –26% mass relative to precursors. Mass losses of Na, K, Ca, Rb, Sr, Cs, Ba and volatiles were –30 to –60% and resulted from the destruction of white mica. Si was depleted from most selvages and transported locally to adjacent veins; average selvage Si losses were about –50%. Y and rare earth elements were added due to the growth of monazite in cracks cutting apatite. The mass balance analysis also suggests some addition of Ti occurred, consistent with the presence of rutile and hematite-ilmenite solid solutions in veins. No major losses of Al from selvages were observed, but Al was added in some cases. Consequently, the Al needed to precipitate vein kyanite was not derived locally from the selvages. Veins more than an order of magnitude thicker than those typically observed in the field would be necessary to accommodate the Na and K lost from the selvages during alteration. Therefore, regional transport of Na and K out of the local rock system is inferred. In addition, to account for the observed abundances of kyanite in the veins, large fluid-rock ratios (10^2 – 10^3 m³_{fluid} m⁻³_{rock}) and time-integrated fluid fluxes in excess of $\sim 10^4$ m³_{fluid} m⁻²_{rock} are required owing to the small concentrations of Al in aqueous fluids. It is concluded that the quartz-kyanite veins and their selvages were produced by regional-scale advective mass transfer by means of focused fluid flow along a thrust fault zone. The results of this study provide field evidence for considerable Al mass transport at greenschist to amphibolite facies metamorphic conditions, possibly as a result of elevated concentrations of Al in metamorphic fluids due to alkali-Al silicate complexing at high pressures.

Key words: fluid flow; high-*P* metamorphism; mass transfer; Scotland; veins.

INTRODUCTION

Aluminium is the third most abundant element in the crust, yet its geochemical behaviour in the deep crust during orogenic events is not fully understood. Aluminous minerals such as corundum and the Al₂SiO₅ polymorphs have traditionally been considered to have extremely low solubilities in typical metamorphic fluids based on textural observations (e.g. Carmichael, 1969) and mineral-H₂O experiments (e.g. Anderson & Burnham, 1967; Burnham *et al.*, 1973; Ragnarsdottir & Walther, 1985). However, the presence of kyanite and other Al₂SiO₅ polymorphs in veins and altered

rock adjacent to veins indicates some degree of Al mobility during metamorphism (see Kerrick, 1990 for a review; Chinner, 1961; Ague, 1995; Nabelek, 1997; Whitney & Dilek, 2000; Widmer & Thompson, 2001; Putlitz *et al.*, 2002; McLelland *et al.*, 2002; Larson & Sharp, 2003; Sepahi *et al.*, 2004; Allaz *et al.*, 2005; Beitter *et al.*, 2008). Furthermore, recent experimental data have shown that Al transfer may occur in response to fluid-mineral equilibration under evolving metamorphic conditions (Verlaguet *et al.*, 2006) and that Al-Si-Na complexing facilitates a significant increase in dissolved Al as Si and Na increase in solution (Manning, 2006, 2007; Tropper & Manning,

2007; Newton & Manning, 2008). Such complexing could facilitate considerable fluid-driven transport of Al, yielding a plausible explanation for the occurrence of Al_2SiO_5 polymorphs in and around veins in metamorphic rocks (cf. Manning, 2007).

Veins are mineralized fractures that mark regions of mass transfer in metamorphosed rocks, yet fundamental questions surround the nature and scale of mass transfer, particularly for Al. The mass precipitated in veins is derived from the fluid flowing through fractures, the surrounding wall rocks or a combination of the two (e.g. Ferry & Dipple, 1991; Yardley & Bottrell, 1992; Ague, 1994b; Widmer & Thompson, 2001; Molina *et al.*, 2004). Field studies of metamorphic veins have reached differing conclusions about the processes of Al transfer. For example, some studies infer transport of Al by regional fluid flow, associating Al mobility with large channelized fluid fluxes (Ague, 2003a) or typical regional fluxes arising from the devolatilization of metasediments (Beitter *et al.*, 2008). Other studies provide evidence that the Al needed to form vein kyanite can be derived locally from adjacent wallrocks by diffusion through a pore fluid phase (Widmer & Thompson, 2001). Clearly, the nature and amount of transfer will depend on many geological variables, including the P - T - t history of metamorphism, the fluid compositions and fluxes, and the chemical compositions of the rock units involved.

The Dalradian Saxa Vord Pelite in the north-east corner of the Island of Unst in the Shetland Islands (Scotland; Fig. 1) contains numerous syn-metamorphic quartz-kyanite veins (Figs 2 & 3) and is ideal for the study of fluid flow and mass transfer of Al and other elements. These veins are particularly notable for the presence of large splays of kyanite, as described in the classic paper of Read (1932). Furthermore, the veins are surrounded by chemically and mineralogically altered host rock ('selvages'), indicating significant mass transfer between infiltrating fluids and the wall rocks. This study addresses the chemical and mineralogical changes associated with vein and selvage formation, the length scales of fluid flow and element mass transfer, possible fluid sources contributing to vein formation and the implications for Al mobility in deep crustal, orogenic environments. A fundamental objective is to test whether the Al that formed the vein-kyanite was transported regionally by fluids, or whether it was derived more locally from adjacent wall rocks.

GEOLOGICAL BACKGROUND

The Shetland Islands are located north of the Scottish mainland at *c.* 60°N and 1°W (Fig. 1). Unst is the northernmost island and consists largely of metamorphic basement rocks and the structurally overlying

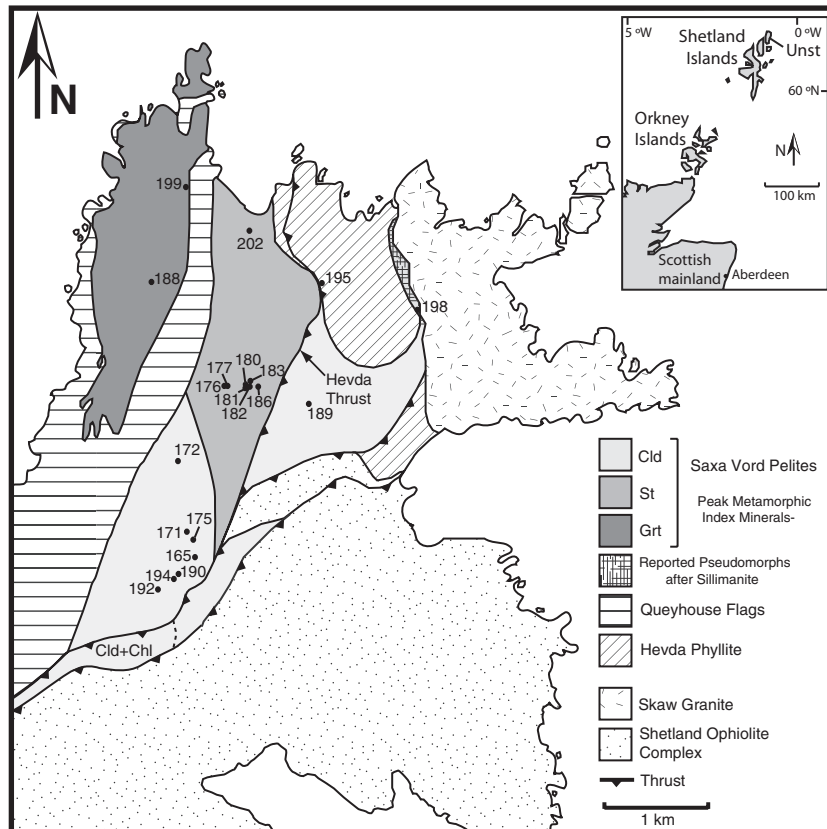


Fig. 1. Simplified geological map of the NE corner of Unst showing major lithological units and structural features. Mineral abbreviations in all figures after Kretz (1983). Sample numbers begin with prefix JAB. Characteristic metamorphic mineral zones based on sampling carried out for this study and Flinn *et al.* (1996). The area where garnet is widespread (dark grey) is referred to by Flinn *et al.* (1996) as the 'East Summit Pelite'. See text for discussion. Modified after British Geological Survey (2002) and Flinn *et al.* (1996).

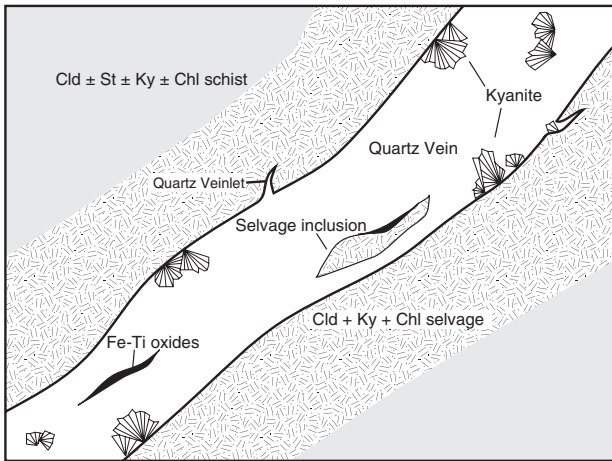


Fig. 2. Sketch of vein, altered selvage and precursor schist relationships. Vein widths typically range from a few centimetres to a few decimetres.

Shetland Ophiolite Complex (Fig. 1). The metapelitic rocks of the study area belong to the Saxa Vord Group, which is composed mainly of three rock units: Saxa Vord Pelite, Hevda Phyllite and Queyhouse Flags. All are inferred to be of Neoproterozoic age, and have been correlated with the Southern Highland Group of the Dalradian in the Scottish Highlands (British Geological Survey, 2002; Flinn, 2007). The quartz-kyanite veins investigated here formed within the Saxa Vord Pelite, largely in the footwall of a regional thrust fault (Hevda thrust). The host rocks are strongly foliated, highly aluminous schists that, at appropriate metamorphic grade, contain chloritoid, staurolite, garnet and kyanite or a combination thereof. Flinn *et al.* (1996) and the British Geological Survey (2002) refer to rocks containing widespread garnet in the north-western part of the field area as 'Summit Pelite'; however, the bulk composition of these rocks is indistinguishable from that of typical Saxa Vord Pelite and, thus, we do not distinguish between the two here. The Saxa Vord Pelite has been interpreted as the northern continuation of the Dunrossness Phyllite of Mainland Shetland, but was metamorphosed at greater pressures (Flinn *et al.*, 1996). The Hevda Phyllite comprises less aluminous metapelites that lack chloritoid but generally contain garnet. The Queyhouse Flags are dominated by quartzofeldspathic and micaceous muscovite + biotite ± garnet schists.

Obduction of the Shetland Ophiolite Complex is thought to have begun at *c.* 500 Ma (Flinn & Oglethorpe, 2005), probably at the onset of subduction during the early stages of the closure of the Iapetus Ocean (Flinn, 2007). The later Scandian Event (425–395 Ma) correlated with the final closure of Iapetus, is characterized by granitic magmatism and continued nappe thrusting on Unst (Flinn & Oglethorpe, 2005; Flinn, 2007). The Skaw Granite (Fig. 1) is an augen-

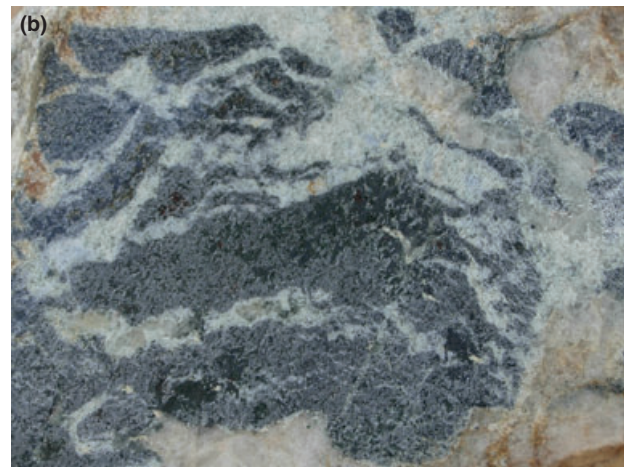
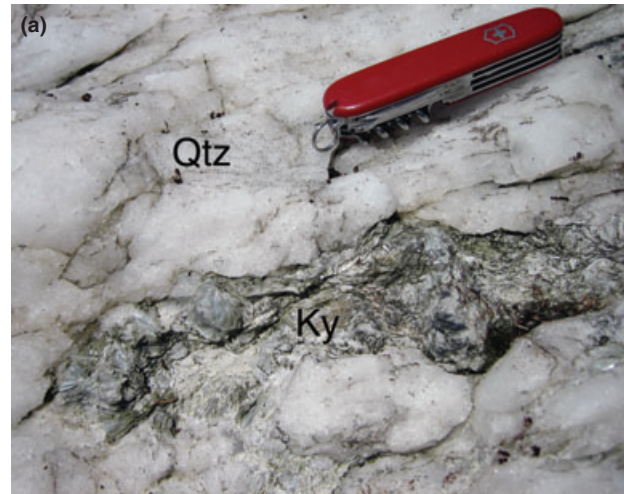


Fig. 3. (a) Outcrop photograph of kyanite in quartz vein (knife is 9 cm long). (b) Photograph of cut rock slab illustrating quartz + kyanite veinlets (light) extending into kyanite + chloritoid + chlorite selvage (dark). Main quartz vein to the right (not in photograph). 10.5 cm wide field of view. Sample JAB195B.

granite that contains rectangular phenocrysts of potassic feldspar reaching 5 cm in length set in a highly foliated matrix of quartz, muscovite, and biotite; muscovite yields an Ar/Ar cooling age of 425 ± 2.6 Ma (Flinn & Oglethorpe, 2005).

Metamorphism

The Saxa Vord Pelite underwent multiple phases of metamorphism (Read, 1932; Snelling, 1957, 1958; Mykura, 1976; Flinn *et al.*, 1996). An early phase produced porphyroblasts that were subsequently pseudomorphed by white mica together with various combinations of chloritoid, kyanite and/or garnet (Fig. 4a,b). Relics of the original minerals are rare in the pseudomorphs. Relic staurolite has been found, and Flinn *et al.* (1996) inferred other minerals including andalusite. In addition, we have observed ovoid pseudomorphs that may have originally been cordierite. This pseudomorph evidence suggests an early

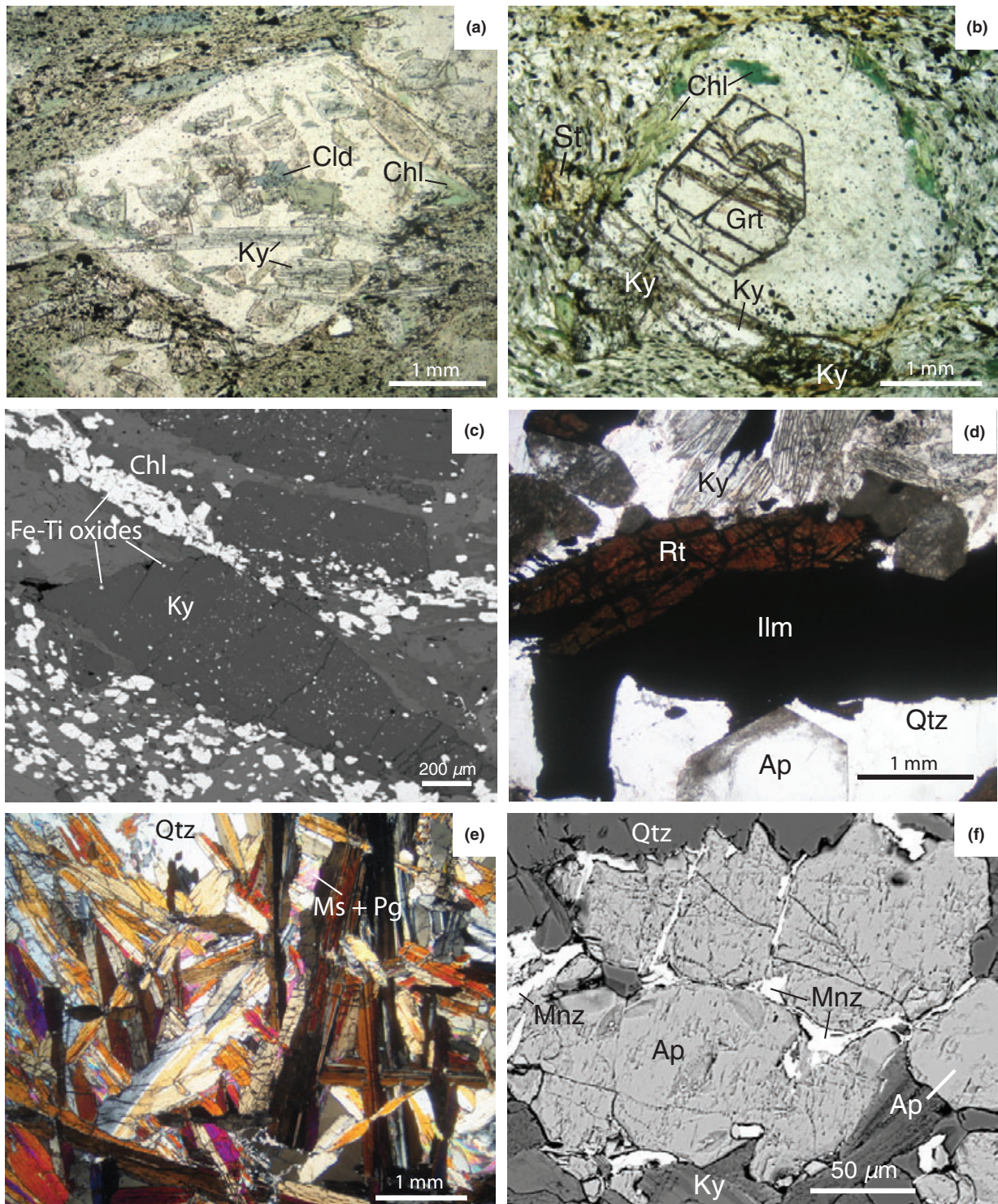


Fig. 4. Representative photomicrographs of typical mineral assemblages. (a) Pseudomorph composed of Cld + Ky + Chl and white mica in selvage sample JAB181E (plane polarized light). Note high percentage of Fe-Ti oxides in the surrounding matrix. (b) Ovoid pseudomorph composed of white mica and garnet porphyroblast, sample JAB188A (plane polarized light). Note the bent kyanite crystal, staurolite and chlorite in surrounding matrix. (c) Back-scattered electron image of selvage sample JAB181A. Note large kyanite crystals with inclusions of Fe-Ti oxides and surrounding bands of chlorite and Fe-Ti oxides. (d) Quartz vein with ilmenite and rutile (partially replaced by ilmenite) as well as large apatite and kyanite crystals from sample JAB176A2 (plane polarized light). (e) Splays of kyanite from vein sample JAB181A. Note minor retrograde growth of muscovite and paragonite around kyanite crystals (cross-polarized light). (f) Back-scattered electron image of fractured apatite crystal with monazite overgrowths in quartz-kyanite vein from sample JAB181A.

phase of relatively low-*P*, but high-*T* metamorphism. A later phase of metamorphism produced a series of index minerals generally indicative of a northerly increase in grade; key index minerals are chloritoid, staurolite and garnet (Fig. 1). Kyanite is widespread, except at the very lowest grades in the southernmost part of the field area. Some rocks were affected by subsequent retrogression (e.g. Mykura, 1976; Flinn *et al.*, 1996). This produced partial to complete chloritization of staurolite, garnet and chloritoid; replacement of staurolite by chloritoid; sericitization of kyanite; and growth of albite at the expense of paragonite. Flinn *et al.* (1996) also reported retrograde white mica-rich 'shimmer aggregate' pseudomorphs after sillimanite near the contact with the Skaw Granite (Fig. 1).

Flinn *et al.* (1996) concluded that porphyroblasts grew during an early phase of regional metamorphism and were then subsequently pseudomorphed. This phase was followed by contact metamorphism due to the intrusion of the Skaw Granite. These authors infer that the widespread chloritoid, kyanite and staurolite in the Saxa Vord Pelite formed as part of a contact aureole around the granite. However, there is no clear spatial relationship between the Skaw Granite and the index mineral zones in the Saxa Vord Pelite, other than the thin band of shimmer aggregate pseudomorphs along the contact. We consider it more probable that a phase of relatively low-*P*, high-*T* metamorphism was followed by a much higher-*P* phase of regional metamorphism that gave rise to the observed distribution of index mineral zones. The absolute ages of the prograde metamorphic events remain to be determined, but they are as old as, or older than, the Skaw Granite. Clearly, major questions remain about the heat sources and the timing of metamorphism in the area. We emphasize, however, that our study of fluid-driven mass transfer is independent of these questions.

METHODS OF INVESTIGATION

Samples were collected from localities chosen on the basis of freshness and proximity to geological features or units of interest. The samples were broadly categorized as precursor host rock far removed from vein alteration, vein selvage or quartz-kyanite vein. The widths of veins and their associated selvages were measured perpendicular to vein-wallrock contacts both in the field and on cut rock slabs. Thin sections were examined optically and with the JEOL JXA-8600 electron microprobe in the Department of Geology and Geophysics at Yale University. Semi-quantitative energy-dispersive spectrometer (EDS) analyses were carried out to constrain Fe-Ti oxide mineral compositions.

Rock samples were prepared for chemical analysis by isolating the portion of interest using a rock saw. The cut surfaces were thoroughly abraded with carbide paper to remove any contamination due to sawing. The samples

were then ultrasonically cleaned in distilled, deionized water. Thirteen precursor, 22 selvage and three quartz-kyanite vein samples were selected based on freshness and geological relationships. Chemical analyses for major and trace elements were carried out by SGS Minerals Services using X-ray fluorescence (XRF) and inductively coupled plasma-mass spectrometer (ICP-MS) techniques (Tables 1 & 2; for a summary of analytical methods and uncertainties, see Ague, 1994a, 2003a). We note that analytical uncertainties are dwarfed by compositional variations resulting from both chemical heterogeneities in the original sedimentary precursors and metasomatic changes.

Pseudosections were constructed for representative precursor schist and selvage bulk compositions using version 15.05.08 of the Theriak/Domino software of Christian de Capitani (de Capitani & Brown, 1987) (<http://titan.minpet.unibas.ch/minpet/theriak/theruser.html>). The Domino program calculates equilibrium assemblage phase diagrams using Gibbs free energy minimization. The thermodynamic data were taken mostly from the internally consistent database supplied with the program. However, the standard enthalpy of formation of Mg-staurolite was adjusted in order to match, as closely as possible, the staurolite stability field of Powell *et al.* (1998) for typical Fe-rich metapelitic bulk compositions. The enthalpy used was $-25072.594 \text{ kJ mol}^{-1}$, and the entropy, molar volume and heat capacity were from Holland & Powell (1998).

MINERAL ASSEMBLAGES AND PETROGRAPHY

Metapelitic schist precursors

Metamorphic grade in the Saxa Vord Pelites increases in a general way to the north. In the south-southwest, the rocks are composed mostly of white mica (muscovite + paragonite \pm margarite), quartz, chloritoid (Cld) and chlorite (Chl). At this and higher metamorphic grades, Fe-Ti oxides (\pm rutile \pm ilmenite-hematite \pm magnetite) are widespread. Kyanite (Ky) is also found, particularly in and around quartz veins. Garnet (Grt) is rare, but mineral assemblages of white mica + quartz + Cld + Grt \pm Chl are locally present. With increasing grade, staurolite (St) appears, chloritoid and chlorite are less abundant, and garnet remains rare. Typical mineral assemblages are St + Cld \pm Chl, Cld + Ky and St + Cld + Ky (all coexist with white mica and quartz). At the highest grades, mm-scale garnet becomes more abundant and there is considerable diversity in the mineral assemblages. Common assemblages include Grt + St + Chl, Grt + St + Ky + Chl, Grt + St + Ky + Cld and Grt + St + Cld \pm Chl (all coexist with white mica and quartz).

Selvages

Selvages around veins are generally < 20 cm in thickness and are composed predominantly of chloritoid,

Table 1. Major oxides, minor oxides, LOI, Rb, Sr, Ba, Zr, Nb and Y^a.

Sample	R.C. ^b	X ^c	SiO ₂	TiO ₂	Al ₂ O ₃	Fe ₂ O ₃	MgO	MnO	CaO	K ₂ O	Na ₂ O	P ₂ O ₅	LOI	Total ^d	Rb	Sr	Ba	Zr	Nb	Y
165A2	0	–	52.0	0.98	26.6	9.63	1.98	0.11	0.46	2.57	1.05	0.09	4.03	99.6	100	107	520	155	15	8
165A3	0	–	56.8	0.89	23.9	10.1	1.48	0.24	0.41	2.14	0.61	0.08	3.45	100.1	86	62	590	119	16	6
171A	0	–	54.0	0.92	25.4	9.43	1.51	0.19	0.55	2.67	1.35	0.16	3.52	99.7	122	142	560	122	16	28
172A	0	–	54.4	0.91	24.6	8.90	1.97	0.14	0.51	2.95	1.34	0.08	4.15	100.0	127	132	660	116	15	7
175Ai	2	–	97.0	0.02	2.44	0.28	0.05	b.d.	0.06	0.07	0.12	b.d.	0.50	100.5	3	4	b.d.	4	b.d.	b.d.
175Aiii	1	–	35.0	1.13	40.3	11.8	2.38	0.34	0.53	2.29	1.41	0.20	4.21	99.6	109	123	470	140	21	30
176A1	1	–	31.1	1.17	38.7	14.0	4.83	0.23	1.86	1.25	0.43	1.31	4.32	99.2	64	59	410	146	12	80
176A2i	1	–	45.4	0.48	43.6	4.15	1.17	0.04	0.44	1.63	0.43	0.29	2.50	100.2	83	49	420	46	10	40
177A	1	–	30.8	2.16	39.1	19.2	1.82	0.52	0.62	1.44	1.15	0.04	3.90	100.8	68	136	350	285	83	47
180B	1	–	28.7	2.48	38.7	22.9	2.00	0.59	0.15	1.48	0.48	0.03	3.11	100.6	74	44	330	321	16	59
181Ai	2	–	84.3	0.10	13.3	0.99	0.06	0.03	0.05	0.1	0.14	0.03	0.61	99.8	5	9	b.d.	16	2	3
181Aii	1	1.25	40.4	0.90	44.8	8.30	1.51	0.13	0.38	1.01	0.30	0.28	2.08	100.2	51	31	240	99	12	45
181Aiii	1	3.75	34.6	1.56	40.8	15.0	3.00	0.27	0.26	0.88	0.26	0.20	2.99	99.8	45	28	210	164	19	39
181Aiv	1	6.25	31.7	1.49	42.3	15.9	3.20	0.42	0.26	1.02	0.28	0.15	3.38	100.1	51	30	270	169	20	39
181C	1	8	31.9	1.81	40.6	15.9	2.92	0.15	0.48	1.85	0.78	0.11	3.39	100.0	86	93	480	225	17	57
181D	1	10	32.9	1.96	38.9	16.4	2.61	0.14	0.46	1.96	0.84	0.10	3.53	99.8	89	101	480	228	18	47
181E	1	12.5	32.6	1.69	38.3	16.1	3.58	0.16	0.47	2.25	0.88	0.16	3.85	100.2	107	104	610	202	14	41
182A	1	–	34.6	1.85	45.3	13.6	1.29	0.04	0.07	1.84	0.56	0.02	2.18	101.4	98	61	380	197	14	49
183A	1	–	45.8	0.56	43.3	5.79	1.18	0.06	0.08	0.73	0.16	0.03	1.65	99.4	35	20	160	70	8	15
186Ai	2 ^e	–	54.5	0.04	41.9	0.84	0.07	b.d.	0.13	0.71	0.25	0.10	1.43	99.9	36	21	150	7	b.d.	6
186Aii	1	1.5	30.8	1.86	37.7	19.7	4.50	0.32	0.40	0.73	0.33	0.23	4.05	100.7	34	33	140	209	10	59
186Aiii	1	3	35.2	1.74	36.7	15.3	2.77	0.17	0.27	2.1	1.10	0.05	4.25	99.7	96	115	480	228	10	45
186Aiv	1	6	37.7	1.44	35.4	12.2	2.33	0.11	0.46	3.28	2.04	0.04	5.25	100.3	145	215	690	196	8	43
186Av	1	9	38.3	1.35	33.9	11.3	2.66	0.09	0.54	3.76	2.50	0.09	5.66	100.2	167	262	800	184	8	41
186B	0	–	54.9	0.93	24.9	9.28	1.04	0.16	0.42	3.36	1.46	0.09	3.41	100	149	151	b.d.	123	14	25
186D	0	–	55.5	0.93	25.2	8.93	1.22	0.17	0.48	2.59	1.26	0.11	3.42	99.8	120	158	650	116	16	28
188A1	0	–	53.5	1.12	25.1	9.53	2.06	0.14	0.31	2.85	1.79	0.12	3.64	100.1	119	156	510	152	15	23
188A2	0	–	52.0	1.10	26.5	9.00	1.84	0.13	0.35	3.04	2.00	0.09	3.84	99.9	127	175	550	164	14	23
189A	1	–	40.2	1.48	32.7	15.5	2.96	0.32	0.14	0.79	0.48	0.07	4.11	98.8	38	33	140	224	22	48
192B	1	–	32.1	1.71	38.2	16.9	1.86	0.60	0.91	1.89	1.58	0.11	4.28	100.2	86	175	460	214	32	43
194A	1	–	33.4	1.63	40.4	14.5	0.98	0.28	1.63	1.92	1.75	0.06	3.77	100.4	85	232	450	208	38	39
195A	1	–	36.1	1.30	41.2	12.3	1.91	0.25	0.35	2.59	0.78	0.16	3.55	100.5	125	78	580	151	17	36
195B	1	–	35.6	1.30	47.2	11.6	1.76	0.08	0.54	0.33	0.20	0.40	2.07	101.1	16	28	50	112	17	111
198A	0	–	51.3	1.23	26.4	9.72	2.31	0.20	0.79	2.23	1.73	0.23	4.24	100.4	83	183	560	188	19	14
199A	0	–	49.7	1.08	30.4	9.06	1.28	0.13	0.60	3.18	1.10	0.14	3.88	100.6	133	159	830	134	11	30
199B	0	–	53.6	0.98	24.9	9.72	1.28	0.08	0.31	3.76	1.65	0.13	3.49	100.0	169	172	680	130	17	20
202A	0	–	52.3	1.00	27.2	9.99	1.31	0.09	0.59	2.95	1.33	0.18	3.41	100.4	140	147	630	118	17	26
202C	0	–	54.7	0.95	25.5	9.32	1.91	0.27	0.44	2.48	1.29	0.13	3.56	100.6	111	135	600	122	11	18

^aAnalyses performed using X-ray fluorescence methods. Rb, Sr, Ba, Zr, Nb and Y concentrations are tabulated in p.p.m., all others are listed in weight per cent. All Fe as Fe₂O₃. LOI, loss on ignition; b.d., below detection.

^bR.C., rock codes: 0, precursor schist; 1, altered selvage near vein; 2, quartz-kyanite vein.

^cJAB181A-E and JAB186A are geochemical traverses that extend across alteration selvages adjacent to quartz veins. X indicates distance (cm) along geochemical traverses measured perpendicularly from vein margin at X = 0 to the centre of the sample.

^dWeight per cent total including Rb, Sr, Ba, Zr, Nb and Y summed as oxides.

^eKyanite-rich mass along vein margin; moderate retrograde alteration to white mica.

kyanite, chlorite, Fe-Ti oxides and white mica. The selvage rocks are distinctly coarser grained than the precursor schists, and contain less white mica and quartz, but more kyanite, chloritoid and Fe-Ti oxides. These textural and mineralogical features were used to distinguish the selvages in the field. The original metamorphic fabric is preserved in a few of the selvages, but it is usually destroyed due to the growth of new minerals. The Fe-Ti oxides are present in wormy bands of individual euhedral crystals and are commonly associated with chlorite (Fig. 4c).

Veins

The Saxa Vord Pelite is characterized by quartz veins that contain kyanite and accessory Fe-Ti oxides, chlorite, apatite and monazite (Figs 3 & 4d–f). The veins range in width from several millimetres to the metre scale; most are a few centimetres to a few decimetres wide. Field observations indicate that outcrops contain several volume per cent to as much as 20%

quartz veins. Veins either cross-cut the prevailing regional schistosity, or are sub-parallel to it. Macroscopic deformation features, including folding and boudinage, are evident in some veins. In thin section, vein quartz generally displays prominent undulose extinction. Kyanite forms large radiating splays of elongate crystals that can measure up to 5 cm long (Fig. 3). The modal abundance of kyanite in veins typically ranges from a few per cent to about 20%, although some nearly pure kyanite veins were observed. Oxides are considerably less abundant than kyanite; where present they are found as elongated, slightly curved crystals or masses of crystals as much as several cm long. Blades of kyanite and, in some rocks, large Fe-Ti oxide grains may be bent and/or fractured. In a few samples, hematite-ilmenite solid solutions grew around earlier formed and fractured rutile (Fig. 4d). Large (200 μm) apatite crystals in or adjacent to veins commonly contain fractures filled by monazite (Fig. 4f). In some rocks, quartz-kyanite veinlets extend out into the adjacent selvages (Fig. 3b).

Table 2. Selected trace elements^a.

Sample	La	Ce	Pr	Nd	Sm	Eu	Gd	Tb	Dy	Ho	Er	Tm	Yb	Lu	Nb	Hf	Ta	Th	Cr ₂ O ₃	Ni	Y
165A2	6.3	14.7	1.89	6.2	1.3	0.30	1.09	0.22	1.63	0.38	1.30	0.23	1.6	0.32	16	5	1.6	13.3	0.02	79	8.5
165A3	7.7	16.1	2.06	7.1	1.4	0.28	1.18	0.23	1.43	0.31	1.07	0.19	1.4	0.25	19	4	1.7	10.2	0.02	64	7.4
171A	61.4	114	14.0	50.3	8.7	1.69	7.74	1.23	6.46	1.24	3.61	0.50	3.0	0.51	18	4	1.6	15.8	0.01	66	31.9
172A	4.0	7.3	0.94	3.5	0.9	0.16	1.00	0.18	1.43	0.33	1.08	0.17	1.2	0.31	17	4	1.5	12.5	0.02	64	7.3
175Ai	20.5	38.2	4.94	18.7	3.5	0.68	2.57	0.28	1.07	0.13	0.21	b.d.	0.2	b.d.	b.d.	b.d.	b.d.	0.8	b.d.	7	2.4
175Aiii	25.7	50.3	6.47	23.1	4.6	1.02	4.77	0.92	5.96	1.28	3.70	0.55	3.6	0.52	23	5	1.6	14.6	0.02	68	32.8
176A1	285	456	56.2	209	36.5	7.19	34.2	4.77	21.7	3.68	8.85	1.19	7.2	1.04	15	5	1.1	9.5	0.02	162	93.8
176A2i	177	281	34.4	126	21.5	4.34	20.7	2.68	11.2	1.74	3.98	0.49	3.0	0.43	12	1	0.6	7.2	0.01	33	48.4
177A	81.2	181	24.0	84.3	15.2	2.74	11.4	1.94	10.8	2.21	6.54	0.93	6.3	0.94	98	9	7.3	37.7	0.04	56	57.2
180B	45.0	87.7	11.4	41.1	8.5	1.96	9.23	1.84	12.0	2.58	7.60	1.14	7.4	1.10	18	10	2.7	35.3	0.04	69	65.6
181Ai	17.0	32.8	3.95	13.7	2.3	0.43	1.73	0.22	0.93	0.16	0.41	b.d.	0.3	0.05	3	b.d.	b.d.	2.3	b.d.	b.d.	3.6
181Aii	193	347	42.7	153	26.8	5.31	24.6	3.17	13.6	2.08	4.95	0.63	3.9	0.57	15	3	0.9	11.4	0.02	44	53.6
181Aiii	123	226	28.4	100	17.8	3.60	15.9	2.27	10.7	1.89	4.90	0.69	4.2	0.62	23	5	1.5	18.6	0.02	82	48.2
181Aiv	99.4	192	23.8	83.2	15.0	2.91	13.0	1.97	10.1	1.76	4.62	0.64	4.1	0.64	23	6	1.4	24.5	0.03	100	44.8
181C	23.8	48.5	6.04	20.9	4.3	1.06	6.25	1.41	10.9	2.52	7.58	1.12	7.3	1.08	19	7	1.2	13.1	0.03	99	67.0
181D	19.6	39.0	4.85	17.8	3.8	0.94	5.32	1.26	9.17	2.17	6.63	0.98	6.4	0.93	20	8	1.1	18.4	0.04	94	56.1
181E	45.7	93.4	11.7	41.0	7.7	1.55	7.19	1.33	8.33	1.82	5.33	0.80	5.2	0.74	16	6	0.8	20.7	0.03	110	47.3
182A	26.7	50.4	6.38	23.0	4.9	1.13	6.1	1.30	9.17	2.08	6.40	0.94	5.8	0.87	17	6	1.2	14.7	0.03	42	57.3
183A	21.5	39.1	4.91	17.8	3.4	0.69	3.36	0.59	3.39	0.72	1.97	0.29	2.0	0.28	8	2	b.d.	5.0	0.01	38	17.7
186Ai	77.6	154	19.3	69.2	11.2	1.98	7.49	0.80	2.46	0.28	0.57	b.d.	0.4	b.d.	b.d.	b.d.	b.d.	1.6	b.d.	14	6.4
186Aii	56.6	101	12.9	48.7	8.5	1.74	9.37	1.67	11.3	2.64	7.46	1.10	7.0	1.03	11	6	b.d.	19.2	0.03	126	66.3
186Aiii	25.3	49.5	6.59	25.3	4.7	1.04	5.47	1.11	8.33	1.80	5.51	0.76	5.0	0.72	11	7	1.0	21.9	0.03	87	46.8
186Aiv	47.8	93.8	11.9	46.4	8.8	1.76	8.16	1.39	8.77	1.97	5.46	0.80	5.1	0.75	9	6	0.7	21.3	0.03	77	47.5
186Av	79.0	150	18.7	72.6	13.1	2.51	11.3	1.64	8.98	1.75	4.53	0.66	4.1	0.63	8	5	0.6	20.9	0.02	85	42.4
186B	13.6	27.1	3.51	12.8	2.8	0.65	3.46	0.74	5.31	1.21	3.46	0.50	3.2	0.48	17	4	1.0	10.7	0.02	52	31.8
186D	85.3	154	18.3	64.8	11.2	2.18	9.76	1.43	7.02	1.24	3.43	0.46	2.9	0.40	17	3	1.0	14.8	0.02	55	30.3
188A1	42.5	74.9	9.54	33.6	6.4	1.27	5.71	0.91	5.04	1.02	3.36	0.54	3.9	0.57	17	5	1.3	14.7	0.02	60	25.3
188A2	37.0	59.2	7.30	25.8	4.8	1.02	4.87	0.79	4.55	0.97	3.16	0.53	3.4	0.53	16	6	1.3	16.9	0.01	56	25.9
189A	105	200	26.9	98.7	18.2	3.49	15.6	2.27	11.2	2.22	6.02	0.85	5.5	0.78	25	7	1.8	21.8	0.02	88	55.6
192B	35.4	67.0	8.38	30.6	5.9	1.28	6.36	1.26	8.47	1.86	5.48	0.84	5.1	0.76	35	7	2.4	23.8	0.03	73	47.7
194A	33.0	68.7	8.97	32.3	6.1	1.25	5.94	1.16	7.36	1.62	4.80	0.69	4.3	0.64	42	6	2.3	22.3	0.03	37	42.5
195A	51.2	91.9	11.2	40.1	7.5	1.52	7.47	1.28	7.71	1.56	4.70	0.68	4.2	0.63	20	5	1.4	15.8	0.02	62	41.5
195B	440	667	76.3	272	42.7	8.68	41.4	5.47	23.7	3.95	8.83	1.07	5.7	0.85	20	4	1.2	11.3	0.02	54	128
198A	37.8	84.0	11.1	38.7	7.0	1.33	5.00	0.74	3.47	0.68	1.92	0.30	2.1	0.33	22	6	1.2	18.1	0.02	63	14.7
199A	143	312	38.7	133	22.6	4.16	14.7	2.04	8.46	1.43	3.46	0.47	3.0	0.41	13	4	0.8	15.9	0.02	47	33.3
199B	8.2	15.4	1.96	7.3	1.6	0.41	2.11	0.46	3.62	0.82	2.50	0.36	2.5	0.36	19	4	1.1	12.4	0.02	68	22.0
202A	15.3	30.1	3.94	14.8	3.0	0.58	2.83	0.57	3.86	1.04	3.50	0.57	3.8	0.57	19	4	1.1	12.9	0.02	68	26.7
202C	11.7	23.2	3.04	10.9	2.2	0.43	2.25	0.49	3.43	0.83	2.44	0.36	2.6	0.37	12	4	1.0	12.8	0.02	76	20.7

^aConcentrations determined using ICP-MS methods except Cr determined using XRF. Values in p.p.m. except Cr₂O₃ in weight percent. See Table 1 for sample rock type codes and distance along traverses for samples.

PSEUDOSECTION ANALYSIS AND *P-T* CONDITIONS

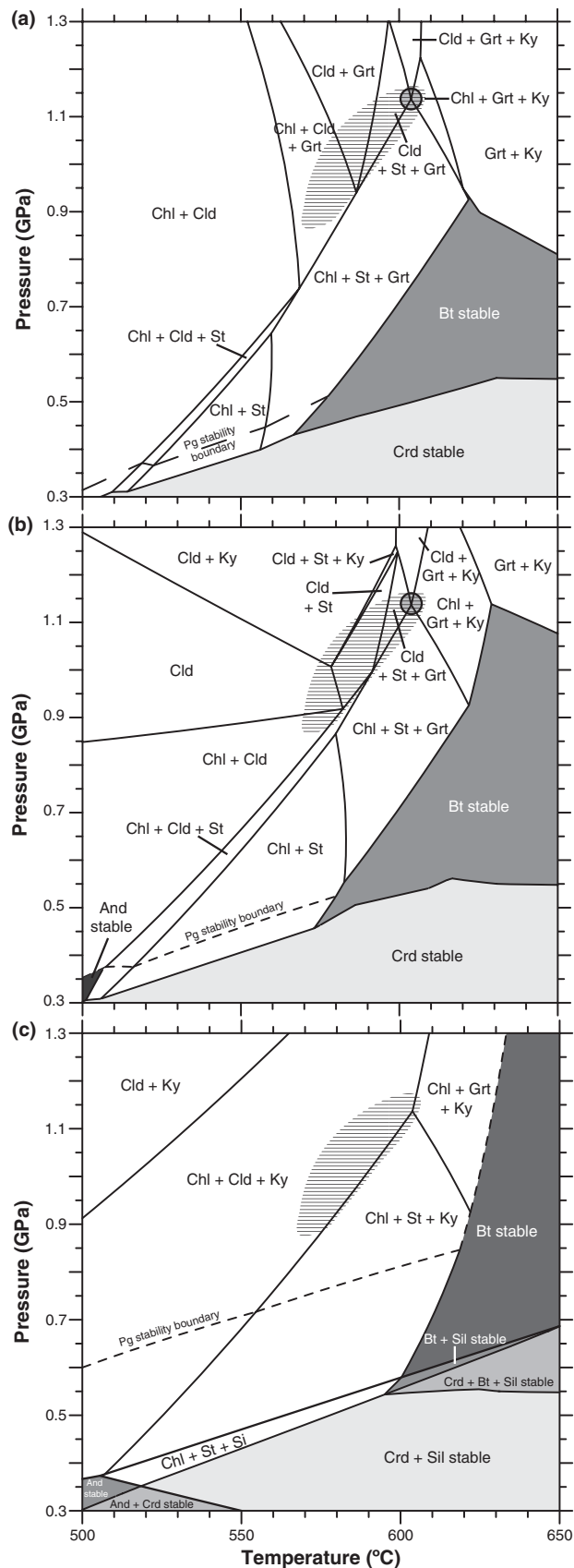
Pseudosections were constructed to assess the *P-T* regime of metamorphism and vein formation. Calculations were performed for the system Na₂O–K₂O–FeO–MgO–Al₂O₃–SiO₂–H₂O (NKFMAH). Although traces of margarite are reported in some rocks (Flinn *et al.*, 1996), CaO was neglected as it is a minor constituent.

Precursor pseudosections

Two pseudosections for the bulk composition of the representative precursor sample JAB165A2 were calculated to investigate the impact of variations in Fe²⁺–Fe³⁺ content on mineral assemblages (Fig. 5a,b). The first pseudosection takes all of the Fe from the XRF analysis to be in the 2+ oxidation state, whereas the second uses 75 mol.% Fe²⁺ and 25 mol.% Fe³⁺ (cf. Flinn *et al.*, 1996). The first pseudosection is intended to represent metapelites poor in hematite-ilmenite and magnetite, whereas the second represents rocks containing greater amounts of oxides. The second pseudosection was constructed using only the ferrous iron because the primary iron-bearing silicates

of interest (Chl, Cld, Grt, St) are all dominated by Fe²⁺. Of course, a wide range of other ferrous/ferric ratios are possible; however, the values used illustrate in a general way how stability fields would be expected to change with composition.

Using the peak mineral assemblages progressing northward through the Saxa Vord Pelite, a metamorphic field *P-T* gradient was constructed. The lowest grade assemblages contain muscovite, paragonite, chlorite, chloritoid and quartz. At higher metamorphic grades, the destruction of chloritoid typically produced staurolite. In some rocks poor in oxides, assemblages containing Grt + Cld ± Chl grew. At the highest grades, muscovite, paragonite and quartz are found together with amphibolite facies mineral assemblages including Grt + St + Chl, Grt + St + Ky + Chl and Grt + St + Cld ± Chl. These assemblages are stable in and around the AFM invariant point assemblage Grt + St + Cld + Ky + Chl at about 605 °C and 1.15 GPa (Fig. 5). We note that these invariant point conditions are comparable to those of Powell *et al.* (1998). In fact, our petrographic observations indicate that the AFM invariant assemblage Grt + St + Ky + Cld + Chl may even have formed, although the textural interpretation of the relative timing of chlorite formation, whether



prograde or retrograde, is somewhat ambiguous. It is concluded that the peak conditions were reached near the invariant point at high pressures. Overall, the progression of mineral assemblages in the temperature range of 550–600 °C and a pressure range of 0.8–1.1 GPa (lined region in Fig. 5). Peak pressures of 1.1 GPa indicate crustal depths of about 40 km during metamorphism.

The biotite stability field is shown as an upper temperature limit as biotite is not found. The cordierite stability field is located at lower pressures. The absence of cordierite from amphibolite facies Saxa Vord Pelite indicates that regional metamorphic pressures were in excess of 0.5–0.6 GPa. If some of the pseudomorphs were originally cordierite, the early phase of metamorphism took place at or below these pressures.

Selvage pseudosection

A pseudosection for the representative selvage sample JAB181Aiii was also calculated (Fig. 5c). The selvages generally have a greater modal abundance of Fe-Ti oxides than the precursor schists. Using the modal amount of hematite-ilmenite solid solution together with the mole percentage of hematite (75 mol.%) calculated from electron microprobe analysis, the appropriate amount of ferric iron associated with hematite-ilmenite solid solutions was then calculated and subtracted from the total iron. The resulting value was assumed to be the amount of ferrous iron in the sample. The pseudosection was calculated using only ferrous iron, which is reasonable considering that chloritoid and chlorite, the primary iron-bearing silicate minerals in the selvages, are dominated by Fe^{2+} .

Across all metamorphic grades the selvages contain chloritoid, kyanite, muscovite, paragonite, chlorite and quartz. This mineral assemblage defines a large stability field bounded at high temperatures by the assemblages $\text{Chl} + \text{St} + \text{Ky}$ and $\text{Chl} + \text{Grt} + \text{Ky}$ (Fig. 5c; garnet and staurolite are not observed in the selvages). The selvages contain considerably less K and Na and more Al than precursor schists far removed from veins. These chemical relationships expand the stability field for the

Fig. 5. NKF MASH P - T pseudosections for representative precursor and selvage compositions. All equilibrium assemblages also contain $\text{Ms} + \text{Pg} + \text{Qtz} + \text{H}_2\text{O}$, except for those below the paragonite stability field, which lack paragonite. Simplified biotite, cordierite, andalusite and sillimanite stability fields are shown for reference. The grey circle indicates the P - T invariant point where $\text{Chl} + \text{Cld} + \text{St} + \text{Grt} + \text{Ky}$ coexist. The P - T metamorphic field gradient is shown as the lined area. (a) P - T pseudosection calculated using the composition of precursor sample JAB165A2 assuming that all Fe from XRF analyses was in the Fe^{2+} state. (b) P - T pseudosection calculated using the composition of precursor sample JAB165A2 assuming that 75 mol.% Fe from the XRF analyses was in the Fe^{2+} state and the remainder was in the Fe^{3+} state. (c) P - T pseudosection calculated using the composition of selvage sample JAB181Aiii.

highly aluminous assemblage Chl + Cld + Ky in selvages relative to precursor schists. Importantly, the range of prograde P - T conditions inferred from the precursors falls within the Chl + Cld + Ky stability field calculated for the selvages.

MASS TRANSFER RELATIONSHIPS

The mobility of 'non-volatile' rock-forming elements during regional metamorphic fluid flow has been demonstrated by the examination of metamorphic veins and their associated alteration selvages (e.g. Ague, 1994a,b; Oliver *et al.*, 1998; Gao & Klemd, 2001; Masters & Ague, 2005; Gao *et al.*, 2007; Penniston-Dorland & Ferry, 2008). The number of such studies, however, remains relatively small and, thus, they are insufficient to constrain the general nature, degree and spatial scale of element mobility and fluid infiltration attending different grades or styles of metamorphism. Consequently, a major goal of this research is to quantify the mass changes between the precursor schists and the selvages to provide new data bearing on processes of metamorphic mass transfer.

Defining a geochemical reference frame

Mass balance methods are used to quantify metasomatism (e.g. Gresens, 1967; Grant, 1986; Ague, 1994a; Baumgartner & Olsen, 1995; Ague & van Haren, 1996). Reference elements are relatively immobile during chemical alteration and are used here to define the geochemical reference frame needed to assess mass changes. Although no element is completely immobile, some have exceedingly low concentrations in solution. Commonly, high field strength elements such as Zr, Ti, Th, and the rare earth elements (REE) are used as

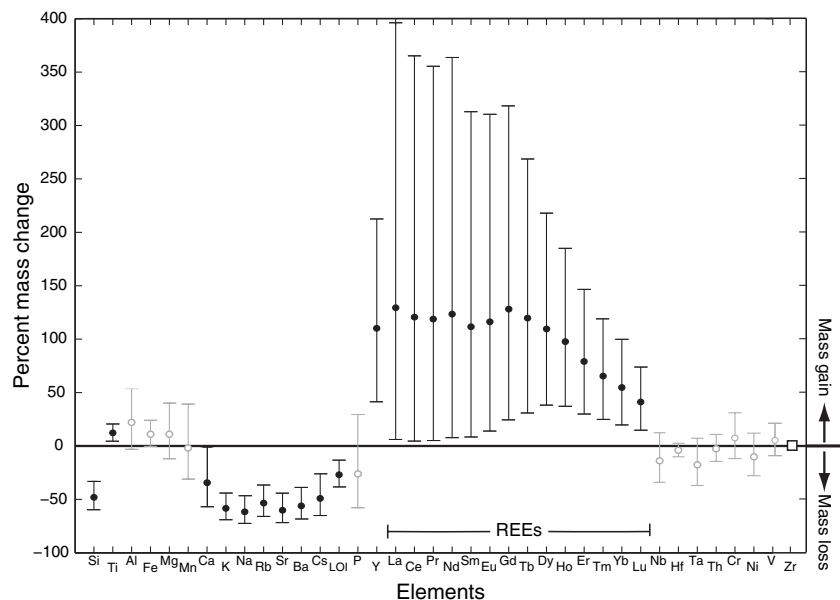
reference species. Nonetheless, great care must be exercised in reference frame selection as each of these elements may be mobile under certain pressure, temperature and fluid composition conditions (e.g. Zeitler *et al.*, 1990; Bröcker & Enders, 2001; Rubatto & Hermann, 2003; Gao *et al.*, 2007).

Monazite grew in cracks cutting apatite grains in and around veins, thus eliminating the REEs as potential reference elements (Fig. 4f). Furthermore, large crystals of ilmenite-hematite solid solutions and rutile within the veins and widespread Fe-Ti oxides in many of the selvage rocks suggest that Ti was mobile as well (Fig. 4d). Zr is predominantly hosted by zircon, which has an extremely low solubility in water-rich metamorphic fluids (Ayers & Watson, 1991; Becker *et al.*, 1999). The fluids were probably H₂O-rich given the absence of carbonate minerals or graphite in the samples. Zircon morphologies varied little across selvage traverses and zircon is absent from vein samples, suggesting that little Zr was added to or lost from selvages during fluid infiltration. The veins contain trace (p.p.m.) levels of Zr, but this Zr would comprise < 1% of the total Zr budget in an outcrop. Thus, Zr was chosen as the reference species to assess mass gains and losses. Nb, Hf, Ta, Th, Cr, Ni and V also typically have small concentrations in metamorphic fluids; as shown below, their geochemical behaviour was identical, within error, to that of Zr (Fig. 6).

Basic equations

The equations used here to quantify mass changes follow Ague (1994a), Ague & van Haren (1996), Philpotts & Ague (2009) and references cited therein. The gain and loss of elements during metasomatism will result in changes in rock mass. For example, 100 g

Fig. 6. Mass percentage change diagram for altered selvages relative to precursors using Zr as a reference element; Nb, Hf, Ta, Th, Cr, Ni and V also appear to have had very limited mobility during metamorphism. Statistically significant (95% confidence level) average mass changes are shown in black; other mass changes in grey open circles. Error bars are 2σ . Note losses of Si, K, Na, Ca, Rb, Sr, Cs, Ba and loss on ignition (LOI – a proxy for volatiles) and gains of Y and REE. Wedge diagrams (Fig. 7) illustrate mass change systematics in more detail, e.g. local mass losses and gains of P, and the addition of Al to some selvages.



of precursor rock could undergo mass transfer such that the final mass is reduced to 80 g. Some elements may have been gained, but these gains were outweighed by the losses of other elements. This kind of overall or total rock mass change ($T_{\text{mass},i}$) calculated using a reference species i is given by:

$$T_{\text{mass},i} = \frac{c_i^0}{c_i'} - 1 \quad (1)$$

$T_{\text{mass},i}$ is a fraction; the percentage mass change can be found by multiplying it by 100. The superscripts 0 and ' indicate the precursor and altered rocks respectively. If rock mass has been lost, then the concentration of i will be greater in the altered rock than in the precursor rock (residual enrichment of i). Conversely, if rock mass has been gained, then the concentration of i will be less in the altered rock than in the precursor rock (residual dilution of i).

The mass change of a mobile species j estimated using species i as a reference is:

$$\tau_i^j = \left(\frac{c_i^0}{c_i'}\right) \left(\frac{c_j'}{c_j^0}\right) - 1 \quad (2)$$

where c_j indicates the concentration of j and τ_i^j is the fractional mass change for j . Uncertainties for Eq. (2) were estimated following Ague (1994a) (also see discussion in Philpotts & Ague, 2009).

Average percentage mass changes

The mass transfer involved in the formation of the vein selvages was evaluated for individual elements by plotting mass percentage changes ($\tau_i^j \times 100$) and their associated uncertainties (Fig. 6). These values represent the average chemical alteration that produced the selvages from the precursor schists during vein formation. On average, the selvages lost Si, Na, K, Ca, Rb, Sr, Cs, Ba and volatiles, and gained Y, REE and Ti. The losses of Si, Na, K, Ca, Rb, Sr, Cs and Ba were very large, ranging from about -30% to more than -60%. Average gains of REEs were considerable, varying from about 115% to 130% for the LREEs and 40% to 130% for the HREEs. Gains of Y in excess of 100% are also indicated. Although the average mass changes for Al and Fe are not statistically significant at the 95% confidence level, mass gains are suggested (see below). In general, mass losses dominated mass gains such that the selvages lost, on average, about -26% total mass relative to precursors ($T_{\text{mass},i} \times 100$).

Wedge diagrams

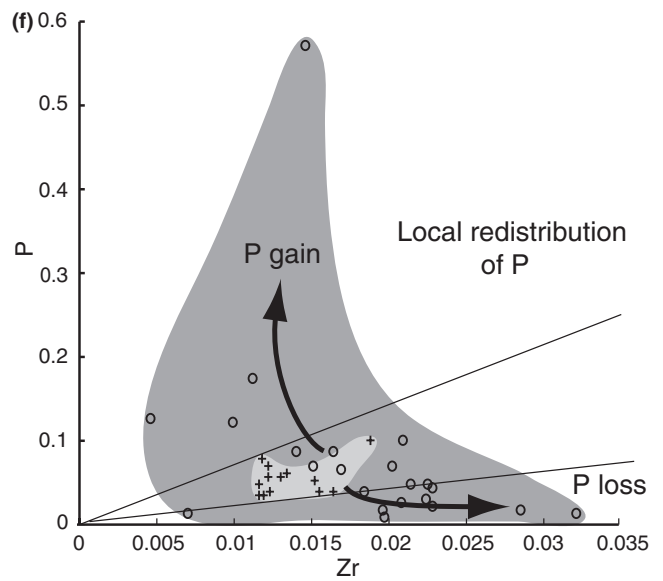
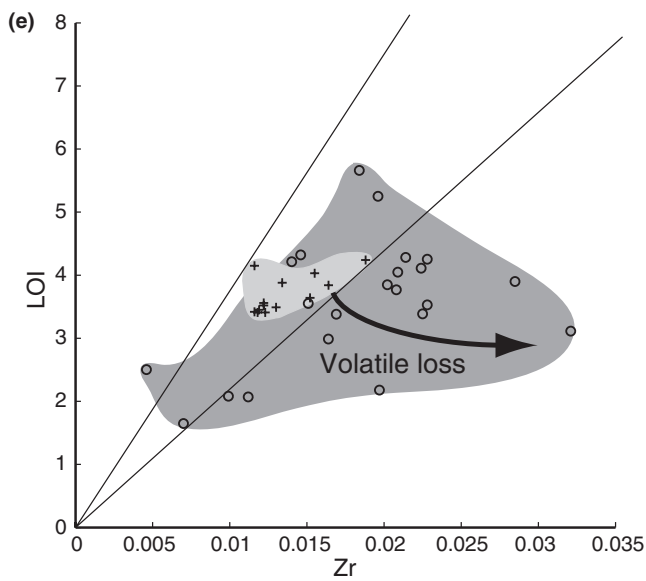
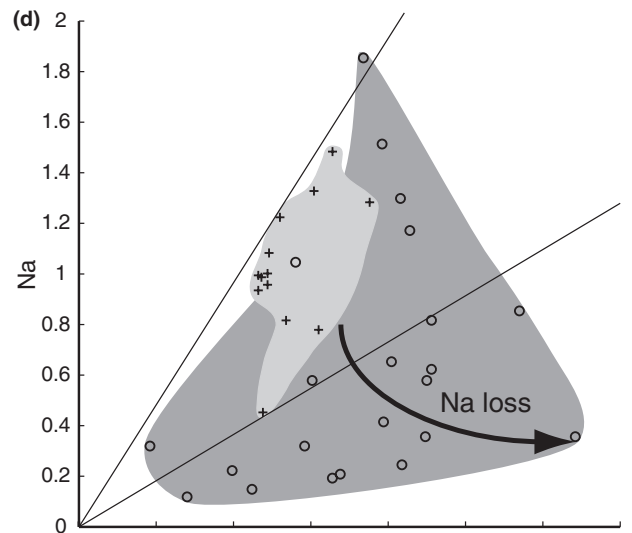
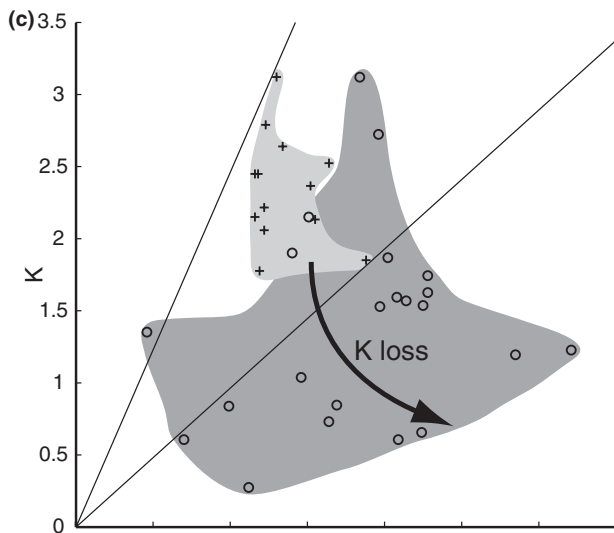
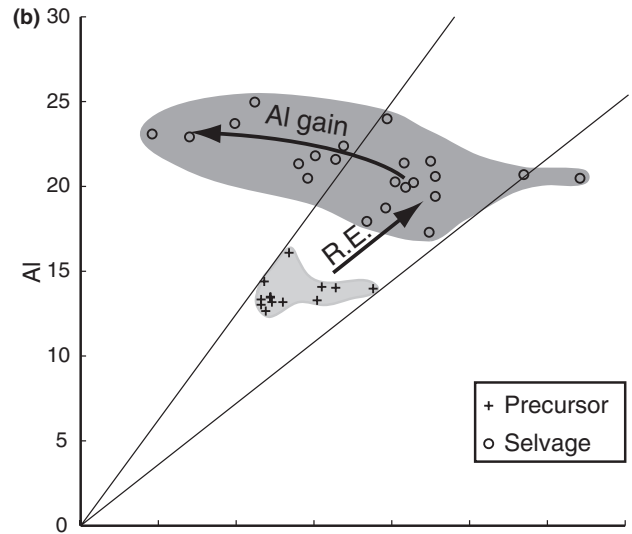
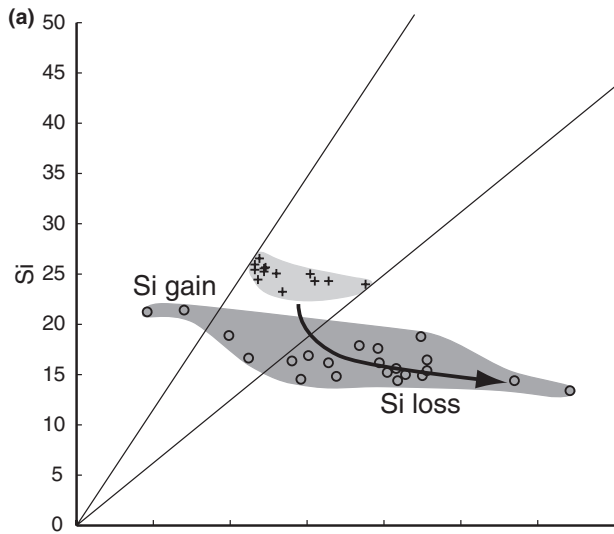
The mass percentage change diagram depicts the average mass changes in individual elements in the selvages, but it does not show variation of individual samples among a population. Plotting the concentration of a potentially mobile element j v. a reference element i for precursor samples will yield a cloud of points because the protoliths in the original sedimentary section were compositionally heterogeneous. The outer edges of this cloud will define a wedge-shaped region that converges on the origin. Selvage samples will plot above the wedge if j was gained, below it if j was lost or within it if j underwent residual enrichment or dilution (Figs 7 & 8; Ague, 1994a; Philpotts & Ague, 2009).

Wedge diagrams for the key constituents Si, Al, Na, K, loss on ignition (LOI – a proxy for volatiles) and P are shown in Fig. 7. Most selvages lost silica to adjacent veins, but a few examples are cross-cut by quartz veinlets and thus gained silica (Fig. 7a). In many selvages, Al simply underwent residual enrichment, due mostly to the loss of silica (Fig. 7b). However, Al was also clearly added in some cases. One selvage sample (180B) plots below the wedge (Fig. 7b). It was collected adjacent to a several cm wide kyanite 'segregation' present in the selvage. For this sample, Al may have been locally transferred into the kyanite segregation, or the low Al/Zr ratio may simply be due to local chemical heterogeneities. However, for most samples, residual enrichment and, in some cases, Al addition, were dominant.

Although there is some scatter in the data, the wedge diagrams clearly indicate overall loss of K, Na and LOI (Fig. 7c–e). Phosphorous was lost from some selvages and gained in others, suggesting local-scale redistribution (Fig. 7f). This variable geochemical behaviour is manifested by the relatively large error bar for P on the mass percentage change diagram (Fig. 6).

Wedge diagrams for relatively immobile elements such as V and Hf are distinctly different than those for highly mobile elements. In most selvages, V and Hf were residually enriched due to overall mass loss; however, residual dilution occurred in a few samples due to mass addition of quartz veinlets (Fig. 8). The only way V, Hf and Zr could have all been mobile is if they all underwent exactly the same amount of mass transfer, a result that would be extremely fortuitous. Similar arguments hold for Nb, Ta, Th, Ni and Cr, all of which show no evidence for net mass loss or gain (Fig. 6).

Fig. 7. Wedge diagrams. The light grey and dark grey areas mark the clouds of precursor and selvage data points respectively. Analytical uncertainties for individual analyses based on replicate chemical determinations are far smaller than variability due to protolith heterogeneities and mass transfer effects. For example, the 2σ standard deviations (wt.%) are ± 0.57 for Si, ± 0.32 for Al, ± 0.15 for K, ± 0.092 for Na, ± 0.72 for LOI, ± 0.015 for P and $\pm 6.8 \times 10^{-4}$ for Zr (Ague, 1994a, 2003a). (a) Si. Most selvages lost silica to adjacent veins, but some examples are cross-cut by quartz veinlets and thus gained silica. (b) Al. In many selvages, Al was residually enriched (R.E.), due mostly to the loss of silica. However, Al was also clearly added to some selvages. (c) K was lost from selvages due to destruction of muscovite. (d) Na was lost from selvages due to destruction of paragonite. (e) Loss on ignition (LOI – a proxy for volatiles). Volatile loss strongly suggests that the selvages formed during prograde metamorphism. (f) P was lost from some selvages and gained in others, suggesting local-scale redistribution.



Geochemical traverses

During metamorphic fluid infiltration rocks adjacent to veins will change composition in order to eliminate chemical potential gradients that arise due to the juxtaposition of a compositionally distinct fluid phase. Geochemical traverses perpendicular to vein-selvage contacts illuminate the magnitude and length scale of this metasomatic alteration. Two geochemical traverses from sample sites 181 and 186A were made (Fig. 9). The thicknesses of the veins adjacent to the 181 and 186A traverses were *c.* 30 and 10 cm respectively.

In both geochemical traverses, Si is depleted in the selvage wall rock (Fig. 9a). The traverses did not span the entire depletion zone for Si as the most distal values are still well below those of the average precursor rock (further sampling was prevented by exposure limitations). Noticeably, however, Si/Zr ratios along the 181 traverse increase approaching the vein, and are larger than those for the more distal samples in the traverse. Because Zr specifies the geochemical reference frame, increases in Si/Zr correspond to Si mass addition. Si addition resulted from the formation of small quartz-kyanite veinlets that extend out from the vein and penetrate as much as 6 cm into the selvage (cf. Fig. 3b).

Al mobility was variable. For the 181 traverse, Al/Zr ratios increase towards the vein, similar to Si/Zr ratios, due to kyanite precipitation in veinlets extending into the selvage (Figs 3b & 9b). On the other hand, no significant changes in the Al/Zr ratio are evident for the 186A traverse, and the ratios are indistinguishable from average precursor values. These relationships suggest that Al, like Zr, was not mobilized to any significant

degree during 186A selvage formation. The wedge diagram indicates that the residual behaviour observed for traverse 186A was somewhat more common than the Al addition observed for 181 (Fig. 7b).

Alkalis (Na, K, Rb) and alkaline earths (Sr, Ba) are depleted from the selvages (Fig. 9c–g). The most distal samples from the vein in traverse 186A have ratios similar to those of the precursors, indicating that the 186 traverse extends across the entire zone of depletion for these elements. In contrast, the ratios for the 181 traverse do not attain precursor values and, thus, the 181 traverse does not extend across the entire width of alteration (due to exposure limitations). For the 181 traverse, the Na/Zr, K/Zr, Rb/Zr and Ba/Zr values directly at the margin of the vein are slightly larger than for the other samples in the traverse due to minor sericitization of kyanite in the selvage closest to the vein (sample 181Aii). This, however, is a retrograde reaction that occurred after the main episode of vein formation and selvage alteration. In spite of the retrogression, ratios for all 181Aii samples are still smaller than the lowermost 2σ sample standard deviation bounds for precursor schists, with the exception of Rb/Zr (Fig. 9c–f). Sr/Y ratios are uniformly low and decrease towards the veins due to the addition of Y and loss of Sr in the selvages (Fig. 9g). In general, REE mass transfer was variable, with some selvages indicating addition and others not (Fig. 9h). This variability accounts for the relatively large error bounds for the REEs on the average mass percentage change diagram (Fig. 6).

Noticeably, the length scales of alteration for the 181 and 186A traverses and for the various elements are

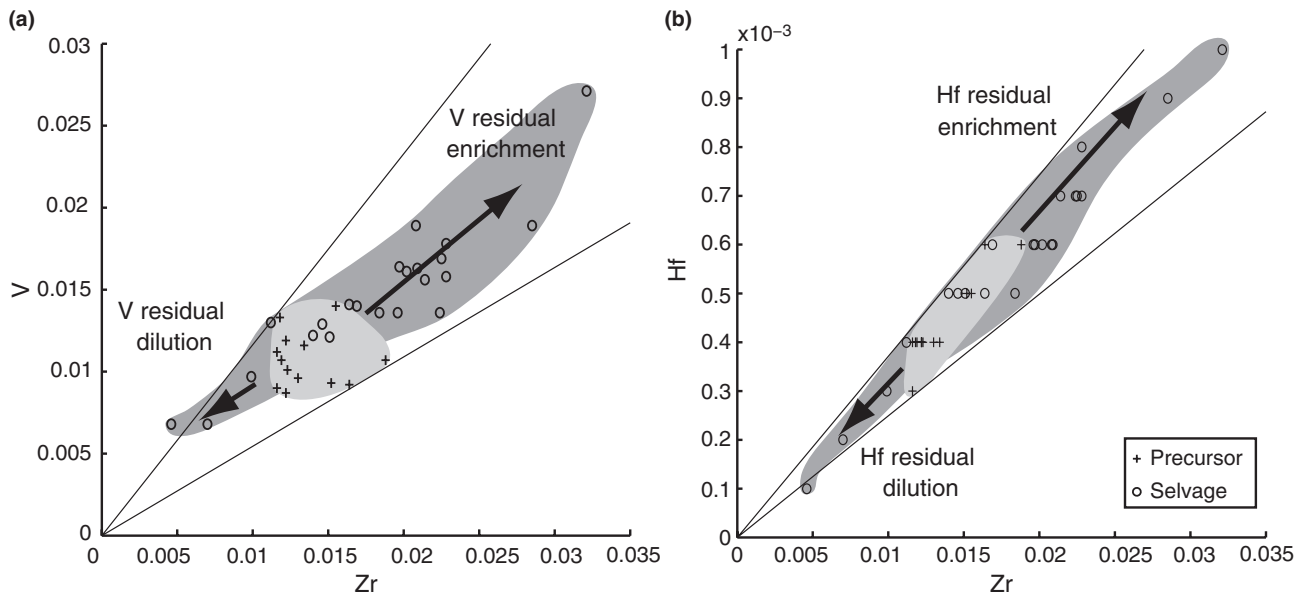


Fig. 8. Wedge diagrams for (a) V and (b) Hf highlighting residual enrichment or residual dilution trends. The light grey and dark grey areas mark the clouds of precursor and selvage data points respectively. Neither V nor Hf underwent significant mass transfer; residual enrichment was due mainly to silica loss, whereas a few samples also underwent silica \pm Al addition leading to residual dilution. The 2σ sample standard deviations for V based on multiple analyses are ± 0.002 wt%. Hf data are reported to the nearest ± 0.0001 wt%.

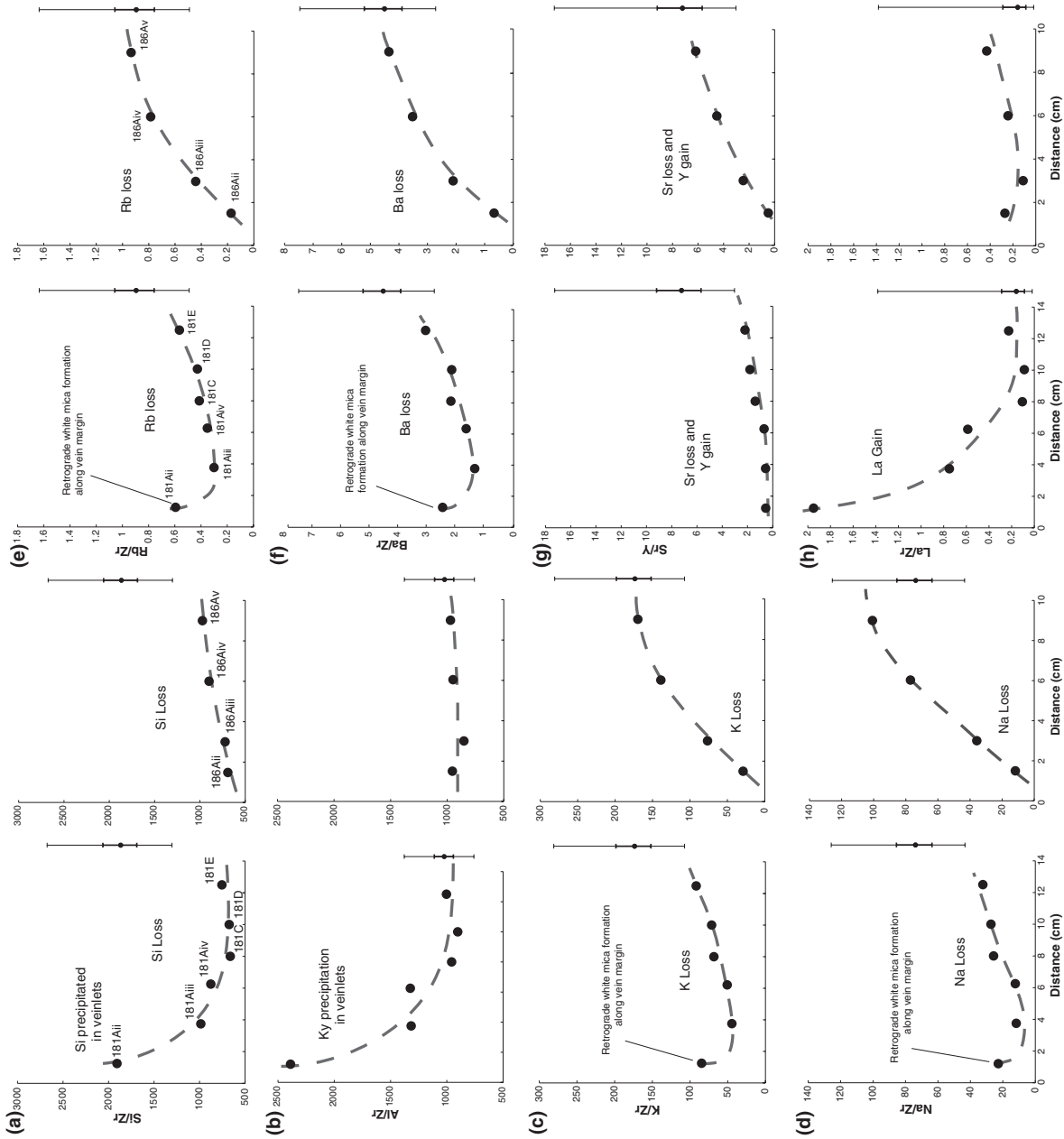


Fig. 9. Geochemical traverses for sample sites 181 and 186. Vein contacts at 0 cm. The geometric mean for precursor samples is indicated with a dot to the right of the right of the traverses. The geometric mean is used because compositional ratio statistics generally do not have Gaussian distributions (cf. Ague, 1994a). Standard deviations (2σ) of the mean and the population are indicated by thick and thin error bars respectively. See text for discussion. (a) Si/Zr. (b) Al/Zr. (c) K/Zr. (d) Na/Zr. (e) Rb/Zr. (f) Ba/Zr. (g) Sr/Y. (h) La/Zr.

different. For example, Si is highly mobile and has the longest length scale of alteration, not attaining precursor values over the extent of both the traverses. Si/Zr and Al/Zr ratios for the 181 traverse are larger proximal to the vein due to the penetration of small quartz-kyanite veinlets (cf. Fig. 3b). Alkali- and alkaline earth-Zr ratios attain precursor values at 8–10 cm for traverse 186A, but are still well below precursor values in traverse 181 at 14 cm.

The vein-selvage relationships of Ague (1994b) and this study indicate that the ratio of the total width of selvage (the sum of the selvage widths on either side of the vein) to the width of the vein varies between roughly 1:1 and 2:1. Therefore, larger veins are expected to have thicker selvages. The vein adjacent to the 181 traverse was *c.* 30 cm thick, whereas the 186A vein was 10 cm thick. As expected, the selvage width and thus length scale of alteration around the 181 vein is greater than for the 186A vein.

Summary of mineralogical changes

Quartz

Most selvage samples lost Si, but it was also added in some cases (Figs 6, 7a & 9a). The bulk of the lost silica is inferred to have been locally transported out of the selvages and deposited as quartz in the adjacent veins. The quartz addition, on the other hand, suggests silica transport at a larger scale by through-going fluids, although some local transport and deposition may have also occurred. The volume percentages of veins across the field area could not be confidently determined due to exposure limitations and, thus, we have not attempted to estimate the total amount of regional silica addition.

Kyanite

The Al wedge diagram indicates that Al was residually enriched in the selvages and also added to some (Figs 7b & 9b). Silica loss from the selvages probably caused most of the residual enrichment. The Al mass gains were due to kyanite precipitation, commonly in veinlets extending into the selvages away from the vein contacts (Fig. 3b). It is interesting that the field of Al addition emanates from the highly residually enriched region of the wedge diagram. This relationship suggests that residual enrichment occurred first, followed by mass addition (Fig. 7b), although other interpretations are possible.

White mica

Na, K, Ca, Rb, Sr, Cs, Ba and volatiles were all lost during the destruction of muscovite, paragonite and margarite in the selvages (Figs 6, 7c–e & 9c–g). Because Al was either residually enriched or gained in most selvages, these losses led to marked decreases in

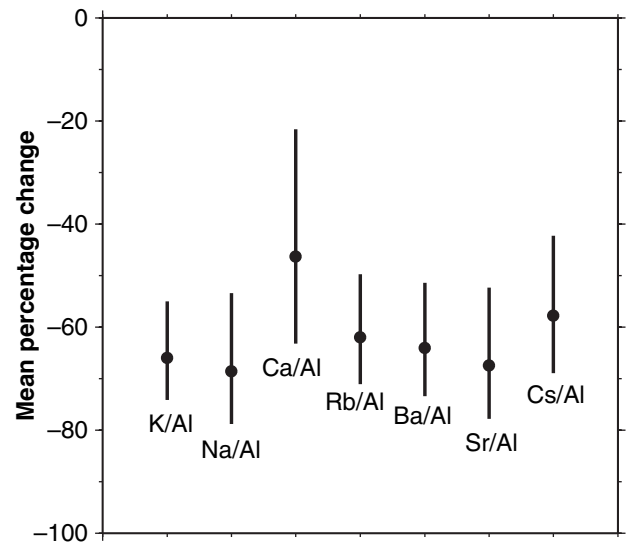


Fig. 10. Mean percentage changes in alkali/Al and alkaline earth/Al ratios between selvages and precursor schists. The negative percentage changes indicate that alkali and alkaline earth metal abundances decreased in the selvages relative to Al as a result of metasomatic alteration adjacent to veins. Uncertainties are 2σ ; statistical calculations follow Ague (1994a).

alkali/Al and alkaline earth/Al ratios (Fig. 10). These decreases, in turn, were essential to stabilize the extremely aluminous Ky + Cld + Chl selvage mineral assemblage. Note that this conclusion is unequivocal because metasomatic changes in *ratios* can be evaluated completely independently of the geochemical reference frame (Zr) chosen for mass balance.

Alkali and alkaline earth metals have been shown to be mobile in metamorphic vein systems in other field studies (e.g. Ague, 1994a,b, 1997, 2003a; Oliver *et al.*, 1998; Breeding & Ague, 2002; Masters & Ague, 2005; Penniston-Dorland & Ferry, 2008). Interestingly, the simple exchange of cations like Na (\pm Ca) for K or *vice versa* cannot explain the geochemical alteration of the selvages of this study. Rather, overall losses of alkalis and alkaline earths occurred.

Monazite, yttrium, phosphorous and REEs

The REEs have traditionally been considered to be relatively immobile during metamorphism (cf. Bau, 1991), but REE transport has now been documented for a number of metamorphic and hydrothermal settings (e.g. Bau & Dulski, 1995; Pan & Fleet, 1996; Whitney & Olmsted, 1998; Boulvais *et al.*, 2000; Ague, 2003a). Gains of Y and REEs in the selvages are consistent with the formation of monazite around apatite grains (Figs 4f & 6). Phosphorous appears to have been locally mobile, added to some selvages and lost from others to form apatite and monazite in and around veins, but it does not display the same mass transfer patterns as Y or REE (Figs 4d,f & 7f). Therefore, P complexes were likely not involved in the

large-scale transport of these elements. Halogen-rich and/or CO₂-rich fluids may transport REEs via fluoride, chloride or carbonate complexing (Gieré & Williams, 1992; Bau & Dulski, 1995; Pan & Fleet, 1996). However, we have not found evidence for major CO₂ or halogen components in the Unst vein fluids. Rather, the association of REE addition with Y addition suggests that REEs may have been transported by Y complexes and then sequestered into monazite (Ague, 2003a). We note that recent studies have shown conclusively that incongruent, fluid-driven breakdown of REE-bearing fluorapatite can locally produce monazite under appropriate conditions (Harlov *et al.*, 2005; Antignano & Manning, 2008a). Nonetheless, our mass balance results show that REE were added to the selvages, ruling out local breakdown of apatite as the only source for the REE in monazite.

Fe-Ti oxides

Some Ti and possibly Fe may have been gained during the formation of Fe-Ti oxides in the selvages and veins (Fig. 4c,d). These findings are consistent with a growing body of evidence for varying degrees of Ti mobility in crustal fluids (cf. van Baalen, 1993; Jiang *et al.*, 2005). Examples include Barrovian settings (Ague, 2003a) and subduction (e.g. Sorensen & Grossman, 1989; Philippot & Selverstone, 1991; Selverstone *et al.*, 1992; Bröcker & Enders, 2001; Franz *et al.*, 2001; Gao *et al.*, 2007).

DISCUSSION

Relative timing of vein and selvage formation

Two major lines of evidence suggest that the veins formed during regional metamorphism at high pressures. First, the selvages lost volatiles, consistent with prograde metamorphic devolatilization, but not retrograde hydration (Figs 6 & 7e). Second, the stability field of Chl + Cld + Ky on the selvage pseudosection lies within the metamorphic field *P-T* gradient that was defined for the precursor schists (Fig. 5). Consequently, the veins and selvages likely formed at or near peak metamorphic conditions. Several other observations are consistent with this conclusion. For example, the selvages contain regional metamorphic minerals, including kyanite and rutile. In addition, the coarse-grained texture of the selvages is suggestive of a fluid-rich, metamorphic environment of formation. If large fluid fluxes occurred during retrograde metamorphism, widespread growth of retrograde minerals, such as albite, would be expected. Last, high pressures enhance the solubilities of aluminous minerals, consistent with the observed widespread mobility of Al (see below). The above findings are not unexpected, as vein formation and regional metamorphism were contemporaneous in many other settings, including the Barrovian garnet zone of the eastern Scottish High-

lands (e.g. Breeding *et al.*, 2004). The above observations, however, do not preclude some degree of veining during exhumation given the broad *P-T* stability field of the selvage mineral assemblage. Veins are observed to cross-cut the regional schistosity and are also commonly deformed themselves. Thus, veining must have taken place after considerable deformation and foliation development, but before deformation ceased.

Local or regional fluid transport?

We first evaluated whether the K and Na lost from the selvages could be accounted for by local redistribution to the veins. To do this, average vein and selvage K₂O and Na₂O contents were used to calculate the thickness of veins necessary to accommodate the K and Na lost from the selvages. These values were then compared with the thicknesses of veins observed in the field. Average vein K₂O and Na₂O contents of 0.085 and 0.13 wt%, respectively, were used based on our two bulk vein analyses (175Ai, 181Ai; Table 1). Representative precursor bulk density ($\rho^0 = 2.80 \text{ g cm}^{-3}$) and selvage bulk density ($\rho' = 2.9 \text{ g cm}^{-3}$) were estimated with the Theriak-Domino software. Mass change calculations (Eq. 2) used average values for precursor/selvage Zr ratio = 0.737, precursor K₂O = 2.83 wt%, selvage K₂O = 1.68 wt%, precursor Na₂O = 1.63 wt% and selvage Na₂O = 0.85 wt%. Average mass losses for K₂O and Na₂O of -58.4 and -61.6%, respectively, equate to mass changes of 0.046 g K₂O and 0.030 g Na₂O lost per cm³ precursor. Changes in rock volume during selvage formation must also be accounted for to ascertain the original volume of rock altered and, therefore, the total amount of K₂O and Na₂O lost. The volume strain using Zr as a reference element was estimated using (Ague, 1994a):

$$\varepsilon_i = \left(\frac{c_i^0}{c_i'} \right) \left(\frac{\rho^0}{\rho'} \right) - 1 \quad (3)$$

where c_i^0 is the average concentration of Zr in the precursor rocks and c_i' is the average concentration of Zr in the altered selvages. The resulting volume strain was -28.9%. Thus, for a typical thickness of 10 cm for selvage on either side of a vein (20 cm total), the original thickness of altered rock would have been about 14 cm (28 cm total), assuming that the strain was perpendicular to vein-wallrock contacts.

The results of the calculations indicate that the observed losses of K₂O and Na₂O from typical decimetre-scale selvages would require veins c. 2–6 m thick (Fig. 11). However, most veins observed in the field were a few tens of centimetres wide or less; a vein of multiple metre-scale thickness was only observed once. Therefore, the necessary vein widths are well over an order of magnitude greater, on average, than observed, requiring considerable transport of these elements out of the rocks over the entire area via regional fluid flow.

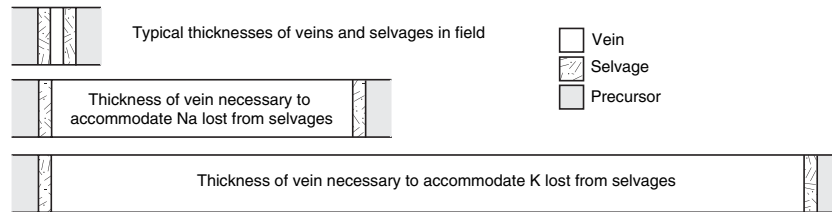


Fig. 11. Sketch of typical decimetre-scale vein and selvage thicknesses observed in the field compared to those necessary to accommodate the Na and K lost from a 10-cm thick selvage on either side of a vein. Required vein thicknesses based on the average vein composition (*c.* 230 and 580 cm for Na and K respectively) are an order of magnitude greater than the thicknesses observed in the field. If the vein analyses are taken individually, the calculated vein thickness ranges are 2.1–2.5 m for Na and 4.7–6.8 m for K.

Al transport and time-integrated fluid fluxes

The mass balance analysis indicates that most of the Al needed to form kyanite in veins was not derived from local wallrocks and must therefore have been transported by advective fluid migration. Given the low concentrations of Al in typical metamorphic fluids, such transport requires large fluid fluxes. Corundum solubility in pure H₂O increases with pressure, but the solubility at 800 °C and 1 GPa is still quite low at 1.3 mmol (Tropper & Manning, 2007), over three orders of magnitude less than that for quartz at equivalent conditions (Manning, 1994). However, complexing with alkalis and/or halides (Diakonov *et al.*, 1996; Tagirov & Schott, 2001; Walther, 2001; Newton & Manning, 2006) and with aqueous silica and/or alkalis (Salvi *et al.*, 1998; Manning, 2007; Newton & Manning, 2008) has been shown to increase the concentration of Al in aqueous solutions at various *P–T* conditions. Indeed, experiments demonstrate that Al concentrations in Si-bearing solutions at 700 °C and 1.0 GPa may reach 5.80 ± 0.03 mmol due to the formation of Al–Si complexes (Manning, 2007). Other experiments indicate that the simultaneous addition of NaCl and SiO₂ to fluids at 800 °C and 1.0 GPa leads to Na-aluminosilicate polymerization and an even greater increase in Al concentrations than either component would produce alone (Newton & Manning, 2008). K-aluminosilicate polymerization is also likely (Wohlers & Manning, 2007). Finally, changes in fluid pH will also strongly affect Al concentrations. Enhanced Al transport by acidic solutions has been widely postulated (e.g. Kerrick, 1990; Nabelek, 1997; McLelland *et al.*, 2002), and higher pH values have also been shown to increase the solubilities of aluminous minerals (Wohlers & Manning, 2009).

The evidence for Al transport in veins can be used to estimate time-integrated fluid fluxes. The following expression describes advective mass transport under local fluid-rock equilibrium (Ague, 2003a):

$$q_{\text{TI}} \approx L \frac{M_e}{\Delta C_e} + L\phi \quad (4)$$

where q_{TI} is the time-integrated fluid flux, L is the characteristic distance of chemical alteration, M_e is the moles of e added (positive) or removed (negative) per

volume rock, ΔC_e is the difference in the concentration of element e between the input and equilibrium fluids (i.e. the concentration drop in moles e per m³ fluid) and ϕ is the porosity. It is assumed that the porosity was relatively small and, thus, the $L\phi$ term is neglected. If the porosity was elevated due to fracturing, the fluid fluxes would have been somewhat larger than those estimated here, but our conclusions regarding significant fluid fluxes would be unchanged. The ratio $M_e/\Delta C_e$ is equivalent to the ‘classic’ fluid-rock ratio, or the volume of reactive fluid that interacted with a unit volume of rock (Bickle, 1992). Given that porosity is thought to be $\ll 1$, a fluid-rock ratio in excess of 1 indicates considerable fluid infiltration. A value of 4.09×10^{-3} mol Al cm⁻³ vein was estimated for M_{Al} using an average vein composition of 7.87% Al₂O₃ (samples 175Ai & 181Ai) and a vein density of 2.65 g cm⁻³. The density of supercritical H₂O at representative conditions of 600 °C and 0.8 and 1 GPa was calculated following Kerrick & Jacobs (1981). Al concentrations in H₂O-rich fluids equilibrated with aluminous rocks are probably in the range of 10⁻² to 10⁻³ M under regional metamorphic conditions (cf. Manning, 2007; Beitter *et al.*, 2008); these values correspond to concentrations of 9.3 to 0.9 mol m⁻³ for quartz-saturated fluids. Thus, the concentration drop ΔC_{Al} caused by kyanite precipitation along the flow path probably fell within this range. Calculation results for the 1 GPa fluid density value (955 kg m⁻³) are shown in Table 3; the 0.8 GPa density value (907 kg m⁻³) yielded only slightly larger flux estimates.

Large fluid-rock ratios of the order of 10² to 10³ were required to form the observed vein kyanite regardless of

Table 3. Calculated time-integrated fluid fluxes^a.

Δm_{Al}^b	ΔC_{Al}^c (mol m ⁻³ fluid)	Fluid-Rock Ratio (m ³ fluid/m ³ rock)	q_{TI}^d for $L = 10$ m	q_{TI} for $L = 10^2$ m	q_{TI} for $L = 10^3$ m
10 ⁻²	9.3	4.4×10^2	4.4×10^3	4.4×10^4	4.4×10^5
10 ^{-2.25}	5.3	7.8×10^2	7.8×10^3	7.8×10^4	7.8×10^5
10 ^{-2.5}	3.0	1.4×10^3	1.4×10^4	1.4×10^5	1.4×10^6
10 ^{-2.75}	1.7	2.5×10^3	2.5×10^4	2.5×10^5	2.5×10^6
10 ⁻³	0.9	4.4×10^3	4.4×10^4	4.4×10^5	4.4×10^6

^aValues calculated for various length scales (L) of Al transport at 1.0 GPa and 600 °C.

^b m_{Al} : molality of Al in supercritical H₂O (mol Al/kg H₂O).

^c C_{Al} : concentration of Al in supercritical H₂O assuming quartz saturation.

^dTime-integrated fluid fluxes (q_{TI}) in units of m³ fluid/m² rock.

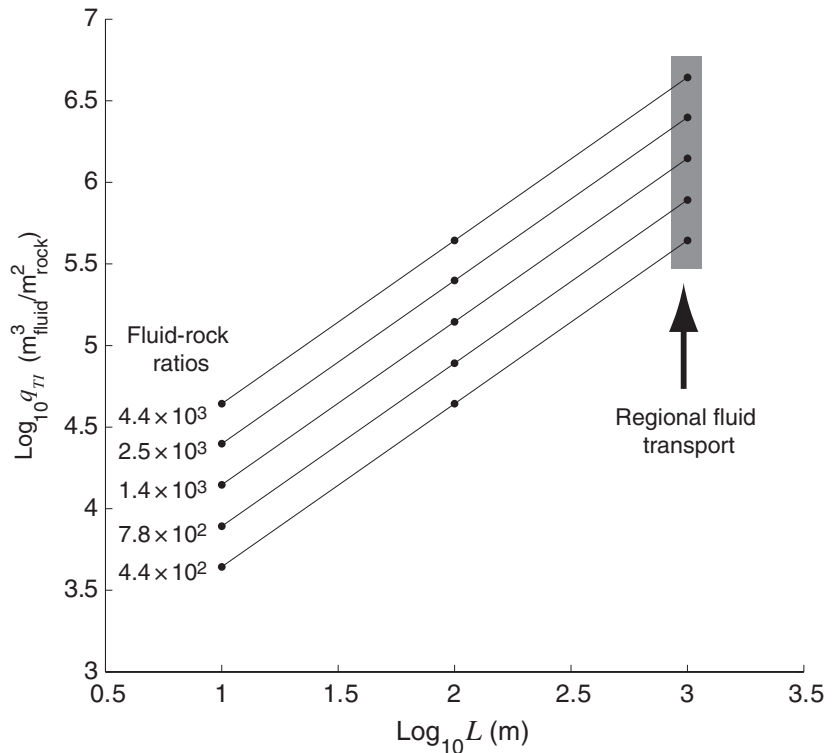


Fig. 12. Calculated time-integrated fluid fluxes v. the characteristic length scale of Al mass transfer (see Table 3). Shaded region indicates time-integrated fluid fluxes for regional-scale transport ($L = 1000$ m).

the value of L (Table 3). The regional distribution of veins on Unst indicates a probable value for L of 100–1000 m, suggesting that time-integrated fluid fluxes could have easily reached 10^5 – 10^6 $\text{m}^3_{\text{fluid}} \text{m}^{-2}_{\text{rock}}$ (Eq. 4; Table 3; Fig. 12). Fluxes of this magnitude through individual veins would have precipitated considerable quartz as well as kyanite, and are similar to fluxes estimated for veins in a number of other metapelitic rocks, including the Wepawaug Schist, Connecticut (3×10^5 $\text{m}^3_{\text{fluid}} \text{m}^{-2}_{\text{rock}}$; Ague, 1994b), the Otago Schist, New Zealand (5×10^6 $\text{m}^3_{\text{fluid}} \text{m}^{-2}_{\text{rock}}$; Breeding & Ague, 2002), and the Waits River Formation, Vermont (4 – 9×10^5 $\text{m}^3_{\text{fluid}} \text{m}^{-2}_{\text{rock}}$; Penniston-Dorland & Ferry, 2008). The L and thus q_{Ti} values would be overestimated if Al was lost locally from the selvages. As illustrated by silica, such losses would be easily identifiable on wedge diagrams (Fig. 7a). However, significant Al loss is not apparent on the Al-Zr wedge diagram (Fig. 7b); in fact, some selvages underwent mass gains.

The cause of kyanite precipitation is unknown, but possibilities include variations in temperature, pressure, pH and fluid composition along the flow path (e.g. Manning, 2006, 2007; Beitter *et al.*, 2008). The fluids that deposited the veins on Unst were saturated in Si and contained dissolved Na and K as well. The enhanced solubility of Al-complexes at high pressures in Si- and alkali-bearing fluids could explain the abundant kyanite in the veins and the enrichment of Al in some of the selvages, as well as the transport of alkalis out of the system.

In addition to kyanite, the presence of rutile and Fe-Ti oxides in veins indicates Ti mobility (Fig. 4d). A recent experimental study has demonstrated that Ti-complexing with dissolved Na-Al silicates in an H_2O -rich fluid phase at mid- to deep-crustal conditions can enhance rutile solubility and transport (Antignano & Manning, 2008b). Although some controversy exists regarding the solubility systematics of rutile, Ti concentrations in aqueous fluids with or without dissolved Na-Al silicates are low, of the order of 10^{-4} – 10^{-5} m at 1.0 GPa and 600 °C (Ayers & Watson, 1993; Antignano & Manning, 2008b). Consequently, time-integrated fluid fluxes must have been large to transport significant quantities of Ti, consistent with the large fluxes estimated based on Al mass transfer. The dissolved Si, Al and alkalis present in the fluids that formed quartz veins during high- P metamorphism of the Saxa Vord Pelite would have facilitated complexing and Ti mobility during fluid-rock interaction.

Other recent studies have addressed the question of how much fluid is necessary to form systems of quartz-kyanite veins. Beitter *et al.* (2008) proposed that the quartz-kyanite veins of the Alpe Sponda in Switzerland were formed by large volumetric fluid-rock ratios of *c.* 1500. They argued that the vein mass was not locally derived and thus must have been precipitated from migrating fluids. Ratios of 1500 are comparable to our intermediate estimates for the quartz-kyanite veins of Unst (Table 3; Fig. 12). Importantly, Beitter *et al.* (2008) calculated their fluid-rock ratio using a somewhat different method

than used here and, thus, the agreement between our two studies is encouraging. However, Beitter *et al.* (2008) concluded that large fluid fluxes were not necessary to precipitate the Alpe Sponda veins, and that typical regional metamorphic devolatilization would have been adequate. It is useful in this context to examine the distinctions between fluid-rock ratios and time-integrated fluid fluxes.

The time-integrated fluid flux generated at the top of a 10 km thick, dehydrating metapelitic sequence will be of order $10^3 \text{ m}^3 \text{ m}^{-2}$ (see review in Ague, 2003b). This quantity is very different than the volumetric fluid-rock ratio (cf. Bickle, 1992). The volumetric fluid-rock ratio can be thought of as the volume of fluid that has reacted with the rock, not the total volume of fluid that has passed through the rock. As a result, such fluid-rock ratios are different for different elements or isotopic tracers, leading to considerable confusion in the literature. Conversely, the time-integrated fluid flux refers to the total amount of fluid that has passed through a rock over a unit area. As shown by Ferry & Dipple (1991), the q_{TI} values needed to precipitate quartz veins by fluid flow down typical temperature and pressure gradients are immense, of order $10^6 \text{ m}^3_{\text{fluid}} \text{ m}^{-2}_{\text{rock}}$ or larger. As a consequence, a typical regional devolatilization flux of $10^3 \text{ m}^3_{\text{fluid}} \text{ m}^{-2}_{\text{rock}}$ would only produce about 0.1 vol.% or less of quartz veins, provided that all the flux was channelized into the veins. Connolly & Thompson (1989) obtained a similar result; their modelling showed that typical regional fluid fluxes are insufficient to precipitate significant amounts of quartz veins.

Our results indicating large fluid-rock ratios and q_{TI} values for vein formation are actually fully consistent with the Beitter *et al.* (2008) volumetric fluid-rock ratio. To estimate the q_{TI} required to precipitate the Alpe Sponda veins, the vein fluid-rock ratio of $c. 1500 \text{ m}^3_{\text{fluid}} \text{ m}^{-3}_{\text{rock}}$ must be multiplied by the length scale of flow (Eq. 4). Taking a representative regional length scale of 1000 m yields a time-integrated fluid flux of the order of $10^6 \text{ m}^3_{\text{fluid}} \text{ m}^{-2}_{\text{rock}}$, a large value consistent with our estimates (Table 3; Fig. 12).

Of course, not all quartz-kyanite veins need have formed due to major fluid infiltration. Widmer & Thompson (2001) concluded that kyanite in veins cutting eclogite facies metabasalts of the Zermatt-Saas zone, Switzerland, formed due to local diffusion of Al from wallrocks into fractures through an essentially stagnant pore fluid. Clearly, much work remains to unravel the geological factors that lead to large-scale transport of Al in some settings, and not in others.

Possible sources of fluid

The vein-forming fluids could have been derived from several possible source regions. The mafic-ultramafic ophiolite complex of Unst is an unlikely source due to the lack of enrichment in Mg, Cr or Ni in the selvages.

The Skaw Granite is also not likely as it contains K-feldspar and plagioclase; fluids derived from or equilibrated with the granite would have been relatively alkali-rich, inconsistent with the observed widespread alkali loss from selvages. However, heat associated with intrusion of the granite may have stimulated fluid flow in the surrounding schists. The Queyhouse Flags are muscovite-rich and plagioclase-bearing and are thus an unlikely source for fluids that would destroy white mica and remove K and Na from the rocks. Although none of these potential fluid origins seems probable, one possibility is that the fluids had travelled far enough away from their source(s) so that they had essentially equilibrated with the Saxa Vord Pelite at the present level of exposure. This scenario, however, is unlikely because of the close proximity of all the rock units to the Saxa Vord Pelite. For example, the contact with the Skaw Granite is at most 2–3 km distant from most of the sample sites, and sample JAB198A, taken directly adjacent to the contact, does not appear to have any potassic or sodic alteration.

An alternative source is the devolatilization of the rock unit itself or deeper metapelitic rocks underlying the Saxa Vord Pelite. Downward fluid fluxes and major convective fluid circulation in the deep crust are considered unlikely (Lyubetskaya & Ague, 2009). Consequently, the fluid fluxes responsible for vein formation on Unst would require the focusing of predominantly upward fluid flow from a larger source region (e.g. a thick sequence of devolatilizing metasedimentary rocks) into a relatively small volume of veined rock characterized by elevated permeability. It is possible that the Hevda Thrust, an ancient fault system or shear zone, was marked by high levels of permeability and acted as a structural control to focus fluids (cf. Dipple & Ferry, 1992). After a fracturing episode, migrating fluids would have deposited some quartz and kyanite in the fractures and driven the chemical alteration of selvages, including the loss of K and Na. With time, the fractures were sealed by local transport of silica from selvages to veins; thus, the veins contain both externally and locally derived quartz (cf. Ague, 1994b). This ‘crack–flow–seal’ process (Ague, 2003b) was likely repeated many times to form the observed vein network.

CONCLUSIONS

Using quantitative mass transfer relationships, we demonstrate that the interaction of fluids and surrounding wall rocks during the metamorphism of the Saxa Vord Pelite drove considerable mass transfer. Si, volatiles, alkalis and alkaline earths were lost from vein selvages, whereas Ti, Y and REEs were gained. Al was residually enriched and, in some cases, added to selvages, indicating that the selvages were not the source of Al for the vein-kyanite and that Al mass

transport was a regional, not local, phenomenon. High-*P* conditions (0.8–1.1 GPa), as inferred from pseudosections, enhanced rutile solubility and contributed to increased Al concentrations in fluids through Na-Al-silicate complexing, thus facilitating the transport of Al and Ti. Regional transport of Na and K out of the local rock system is inferred from mass balance calculations involving the volume of vein necessary to accommodate all the Na and K lost from the selvages during alteration. Large time-integrated fluid fluxes through the fractures ($> \sim 10^4 \text{ m}^3_{\text{fluid}} \text{ m}^{-2}_{\text{rock}}$) and correspondingly large fluid-rock ratios ($10^2\text{--}10^3 \text{ m}^3_{\text{fluid}} \text{ m}^{-3}_{\text{rock}}$) are necessary to account for the geochemical alteration in the selvages and the precipitation of kyanite in the veins. Such large fluxes are indicative of regional fluid focusing along conduits and cracks. Transient periods of elevated permeability related to fracturing episodes along the Hevda thrust fault zone could have provided such a fracture network. The mass balance analysis of chemical alteration associated with high-*P* metamorphic fluid infiltration provides evidence for open system fluid flow and regional-scale mass transport of Al and other non-volatile elements.

ACKNOWLEDGEMENTS

We thank M. Y. Andrews for assistance in fieldwork and sample collection, J. O. Eckert for expertise with the electron microprobe, D. M. Rye and R. A. Strachan for their comments on an earlier version of this paper, and C. E. Manning and S. C. Penniston-Dorland for their thorough and constructive reviews. We gratefully acknowledge support from the National Science Foundation Directorate for Geosciences (NSF EAR-0509934). This work stems from C. E. Bucholz's senior B.S. thesis research at Yale University.

REFERENCES

- Ague, J.J., 1994a. Mass transfer during Barrovian metamorphism of pelites, south-central Connecticut. I: evidence for changes in composition and volume. *American Journal of Science*, **294**, 989–1057.
- Ague, J.J., 1994b. Mass transfer during Barrovian metamorphism of pelites, south-central Connecticut. II: channelized fluid flow and the growth of staurolite and kyanite. *American Journal of Science*, **294**, 1061–1134.
- Ague, J.J., 1995. Deep-crustal growth of quartz, kyanite and garnet into large-aperture, fluid-filled fractures, north-eastern Connecticut, USA. *Journal of Metamorphic Geology*, **13**, 299–314.
- Ague, J.J. & van Haren, J.L.M., 1996. Assessing metasomatic mass and volume changes using the bootstrap, with application to deep-crustal hydrothermal alteration of marble. *Economic Geology*, **91**, 1169–1182.
- Ague, J.J., 1997. Crustal mass transfer and index mineral growth in Barrow's garnet zone, Northeast Scotland. *Geology*, **25**, 73–76.
- Ague, J.J., 2003a. Fluid infiltration and transport of major, minor, and trace elements during regional metamorphism of carbonate rocks, Wepawaug Schist, Connecticut, USA. *American Journal of Science*, **303**, 753–816.
- Ague, J.J., 2003b. Fluid flow in the deep crust. In: *The Crust. Vol. 3. Treatise on Geochemistry* (eds Rudnick, R.L., Holland, H.D. & Turekian, K.K.), pp. 195–228. Elsevier, Oxford, UK.
- Allaz, J., Maeder, X., Vannay, J. & Steck, A., 2005. Formation of aluminosilicate-bearing quartz veins in the Simano nappe (Central Alps): structural, thermobarometric, and oxygen isotope constraints. *Schweizerische Mineralogische und Petrographische Mitteilungen*, **85**, 191–214.
- Anderson, G.M. & Burnham, C.W., 1967. Reactions of quartz and corundum with aqueous chloride and hydroxide solutions at high temperatures and pressures. *American Journal of Science*, **265**, 12–27.
- Antignano, A. & Manning, C.E., 2008a. Fluorapatite solubility in H₂O and H₂O–NaCl at 700–9000 °C 0.7–2.0 GPa. *Chemical Geology*, **251**, 112–119.
- Antignano, A. & Manning, C.E., 2008b. Rutile solubility in H₂O, H₂O–SiO₂, and H₂O–NaAlSi₃O₈ fluids at 0.7–2.0 GPa and 700–1000 °C: implications for mobility of nominally insoluble elements. *Chemical Geology*, **255**, 283–293.
- Ayers, J.C. & Watson, E.B., 1991. Solubility of apatite, monazite, zircon, and rutile in supercritical aqueous fluids with implications for subduction zone geochemistry. *Philosophical Transactions of the Royal Society of London Series A*, **335**, 365–375.
- Ayers, J.C. & Watson, E.B., 1993. Rutile solubility and mobility in supercritical aqueous fluids. *Contributions to Mineralogy and Petrology*, **114**, 321–330.
- van Baalen, M.R., 1993. Titanium mobility in metamorphic systems: a review. *Chemical Geology*, **110**, 233–249.
- Bau, M., 1991. Rare-earth element mobility during hydrothermal and metamorphic fluid-rock interaction and the significance of the oxidation state of europium. *Chemical Geology*, **93**, 219–230.
- Bau, M. & Dulski, P., 1995. Comparative study of yttrium and rare-earth element behaviors in fluorine-rich hydrothermal fluids. *Contributions to Mineralogy and Petrology*, **119**, 213–223.
- Baumgartner, L.P. & Olsen, S.N., 1995. A least-squares approach to mass transport calculations using the isocon method. *Economic Geology*, **90**, 1261–1270.
- Becker, H., Jochum, K.P. & Carlson, R.W., 1999. Constraints from high-pressure veins in eclogites on the composition of hydrous fluids in subduction zones. *Chemical Geology*, **160**, 291–308.
- Beitter, T., Wagner, T. & Markl, G., 2008. Formation of kyanite-quartz veins of the Alpe Sponda, Central Alps Switzerland: implications for Al transport during regional metamorphism. *Contributions to Mineralogy and Petrology*, **156**, 689–707.
- Bickle, M.J., 1992. Transport mechanisms by fluid-flow in metamorphic rocks: oxygen and strontium decoupling in the Troi Seigneurs Massif – a consequence of kinetic dispersion? *American Journal of Science*, **292**, 289–316.
- Boulvais, P., Fourcade, S., Moine, B., Gruau, G. & Cuney, M., 2000. Rare-earth elements distribution in granulites-facies marbles: a witness of fluid-rock interaction. *Lithos*, **53**, 117–126.
- Breeding, C.M. & Ague, J.J., 2002. Slab-derived fluids and quartz-vein formation in an accretionary prism, Otago Schist, New Zealand. *Geology*, **30**, 499–502.
- Breeding, C.M., Ague, J.J., Grove, M. & Rupke, A.L., 2004. Isotopic and chemical alteration of zircon by metamorphic fluids: U-Pb age depth-profiling of zircon crystals from Barrow's garnet zone, northeast Scotland. *American Mineralogist*, **89**, 1067–1077.
- British Geological Survey, 2002. *Unst and Fetlar. Scotland Sheet 131. Solid and Drift Geology. 1:50,000*. British Geological Survey, Keyworth, Nottingham.
- Bröcker, M. & Enders, M., 2001. Unusual bulk-rock compositions in eclogite-facies rocks from Syros and Tinos (Cyclades, Greece): implications for U–Pb zircon geochronology. *Chemical Geology*, **175**, 581–603.

- Burnham, C.W., Ryzhenko, B.N. & Schitel, D., 1973. Water solubility of corundum at 500–800 °C and 6 kbar. *Geochemistry International*, **10**, 1374.
- Carmichael, D.M., 1969. On the mechanism of prograde metamorphic reactions in quartz-bearing pelitic rocks. *Contributions to Mineralogy and Petrology*, **146**, 275–285.
- Chinner, G.A., 1961. The origin of sillimanite in Glen Clova, Angus. *Journal of Petrology*, **2**, 312–323.
- Connolly, J.A.D. & Thompson, A.B., 1989. Fluid and enthalpy production during regional metamorphism. *Contributions to Mineralogy and Petrology*, **102**, 347–366.
- de Capitani, C. & Brown, T.H., 1987. The computation of chemical equilibrium in complex systems containing non-ideal solutions. *Geochimica et Cosmochimica Acta*, **51**, 2639–2652.
- Diakonov, I., Pokrovski, G., Schott, J., Castet, S. & Gout, R., 1996. An experimental and computational study of sodium-aluminum complexing in crustal fluids. *Geochimica et Cosmochimica Acta*, **60**, 197–211.
- Dipple, G.M. & Ferry, J.M., 1992. Metasomatism and fluid flow in ductile fault zones. *Contributions to Mineralogy and Petrology*, **112**, 149–164.
- Ferry, J.M. & Dipple, G.M., 1991. Fluid flow, mineral reactions, and metasomatism. *Geology*, **19**, 211–214.
- Flinn, D., 2007. The Dalradian rocks of Shetland and their implications for the plate tectonics of the northern Iapetus. *Scottish Journal of Geology*, **43**, 125–142.
- Flinn, D. & Oglethorpe, R.J.D., 2005. A history of the Shetland Ophiolite Complex. *Scottish Journal of Geology*, **41**, 141–148.
- Flinn, D., Key, R.M. & Khoo, T.T., 1996. The chloritoid schists of Shetland and their thermal metamorphism. *Scottish Journal of Geology*, **32**, 67–82.
- Franz, L., Romer, R.L., Klemd, R. *et al.*, 2001. Eclogite-facies quartz veins within metabasites of the Dabie Shan (eastern China): pressure-temperature-time-deformation path, composition of the fluid phase and fluid flow during exhumation of high-pressure rocks. *Contributions to Mineralogy and Petrology*, **141**, 322–346.
- Gao, J. & Klemd, R., 2001. Primary fluids entrapped at blueschist to eclogite transition: evidence from the Tianshan meta-subduction complex in northwestern China. *Contributions to Mineralogy and Petrology*, **142**, 1–14.
- Gao, J., John, T., Klemd, R. & Xiong, X., 2007. Mobilization of Ti-Nb-Ta during subduction: evidence from rutile-bearing dehydration segregations and veins hosted in eclogite, Tianshan, NWChina. *Geochimica et Cosmochimica Acta*, **71**, 4974–4996.
- Gieré, R. & Williams, C.T., 1992. REE-bearing minerals in a Ti-rich vein from the Adamello contact aureole (Italy). *Contributions to Mineralogy and Petrology*, **112**, 83–100.
- Grant, J.A., 1986. The isocon diagram – a simple solution to Gresens' equation for metasomatic alteration. *Economic Geology*, **81**, 1976–1982.
- Gresens, R.L., 1967. Composition-volume relations of metasomatism. *Chemical Geology*, **2**, 47–65.
- Harlov, D.E., Wirth, R. & Förster, H.J., 2005. An experimental study of dissolution-reprecipitation in fluoroapatite: fluid infiltration and the formation of monazite. *Contributions to Mineralogy and Petrology*, **150**, 268–286.
- Holland, T.J.P. & Powell, R., 1998. An internally consistent thermodynamic data set for phases of petrological interest. *Journal of Metamorphic Geology*, **16**, 309–343.
- Jiang, S., Wang, R., Xu, X. & Zhao, K., 2005. Mobility of high field strength elements HFSE in magmatic-, metamorphic-, and submarine-hydrothermal systems. *Physics and Chemistry of the Earth*, **30**, 1020–1029.
- Kerrick, D.M., 1990. *The Al₂SiO₅ Polymorphs: Reviews in Mineralogy, Volume 22*. Mineralogical Society of America, Washington, DC.
- Kerrick, D.M. & Jacobs, G.K., 1981. A modified Redlich-Kwong equation for H₂O, CO₂, and H₂O-CO₂ mixtures at elevated pressures and temperatures. *American Journal of Science*, **281**, 736–767.
- Kretz, R., 1983. Symbols for rock-forming minerals. *American Mineralogist*, **68**, 277–279.
- Larson, T.E. & Sharp, Z.D., 2003. Stable isotopic constraints on the Al₂SiO₅ 'triple point' rocks from the Proterozoic Priest pluton contact aureole, New Mexico, USA. *Journal of Metamorphic Geology*, **21**, 785–798.
- Lyubetskaya, T. & Ague, J.J., 2009. Modeling the magnitudes and directions of regional metamorphic fluid flow in collisional orogens. *Journal of Petrology*, **50**, 1505–1531.
- Manning, C.E., 1994. The solubility of quartz in H₂O in the lower crust and upper mantle. *Geochimica et Cosmochimica Acta*, **58**, 4831–4839.
- Manning, C.E., 2006. Mobilizing aluminum in crustal and mantle fluid. *Journal of Geochemical Exploration*, **89**, 251–253.
- Manning, C.E., 2007. Solubility of corundum + kyanite in H₂O at 700 °C and 10 kbar: evidence for Al-Si complexing at high pressure and temperature. *Geofluids*, **7**, 258–269.
- Masters, R.L. & Ague, J.J., 2005. Regional-scale fluid flow and element mobility in Barrow's metamorphic zones, Stonehaven, Scotland. *Contributions to Mineralogy and Petrology*, **150**, 1–18.
- McLelland, J., Morrison, J., Selleck, B., Cunningham, B., Olson, C. & Schmidt, K., 2002. Hydrothermal alteration of late- to post-tectonic Lyon Mountain granitic gneiss, Adirondack Mountains, New York: origin of quartz-sillimanite segregations, quartz-albite lithologies, and associated Kiruna-type low-Ti-Fe-oxide deposits. *Journal of Metamorphic Geology*, **20**, 175–190.
- Molina, J.F., Poli, S., Austrheim, H., Glodny, J. & Rusin, A., 2004. Eclogite-facies vein systems in the Marun-Keu complex (Polar Urals, Russia): textural, chemical and thermal constraints for patterns of fluid flow in the lower crust. *Contributions to Mineralogy and Petrology*, **147**, 484–504.
- Mykura, W., 1976. *British Regional Geology: Orkney and Shetland*. Natural Environment Research Council, Institute of Geological Science, Edinburgh.
- Nabelek, P., 1997. Quartz-sillimanite leucosomes in high-grade schists, Black Hills, South Dakota: a perspective on the mobility of Al in high-grade metamorphic rocks. *Geology*, **25**, 995–998.
- Newton, R. & Manning, C., 2006. Activity coefficient and polymerization of silica at 800 °C, 12 kbar, from solubility measurements on SiO₂-buffering mineral assemblages. *Contributions to Mineralogy and Petrology*, **146**, 135–143.
- Newton, R.C. & Manning, C.E., 2008. Solubility of corundum in the system Al₂O₃-SiO₂-H₂O-NaCl at 800 °C and 10 kbar. *Chemical Geology*, **249**, 250–261.
- Oliver, N.H., Dipple, G.M., Cartwright, I. & Schiller, J., 1998. Fluid flow and metasomatism in the genesis of the amphibolite-facies, pelite-hosted Kanmantoo copper deposit, South Australia. *American Journal of Science*, **298**, 181–218.
- Pan, Y. & Fleet, M.E., 1996. Rare earth element mobility during prograde granulite facies metamorphism: significance of fluorine. *Contributions to Mineralogy and Petrology*, **123**, 251–262.
- Penniston-Dorland, S.C. & Ferry, J.M., 2008. Element mobility and scale of mass transport in the formation of quartz veins during regional metamorphism of the Waits River Formation, east-central Vermont. *American Mineralogist*, **93**, 7–21.
- Philippot, P. & Selverstone, J., 1991. Trace-element-rich brines in eclogitic veins – implications for fluid composition and transport during subduction. *Contributions to Mineralogy and Petrology*, **106**, 417–430.
- Philpotts, A. & Ague, J.J., 2009. *Principles of Igneous and Metamorphic Petrology*, 2nd edn. Cambridge University Press, Cambridge, UK.
- Powell, R., Holland, T.J. & Worley, B., 1998. Calculating phase diagrams involving solid solutions via non-linear equations, with examples using THERMOCALC. *Journal of Metamorphic Geology*, **16**, 577–588.
- Putlitz, B., Valley, J.W., Matthews, A. & Katzir, Y., 2002. Oxygen isotope thermometry of quartz-Al₂SiO₅ veins in high-

- grade metamorphic rocks on Naxos Island (Greece). *Contributions to Mineralogy and Petrology*, **143**, 350–359.
- Ragnarsdottir, K.V. & Walther, J.V., 1985. Experimental determination of corundum solubilities in pure water between 400–700°C and 1–3 kbar. *Geochimica et Cosmochimica Acta*, **48**, 159–176.
- Read, H.H., 1932. On quartz-kyanite-rocks in Unst, Shetland Islands, and their bearing of metamorphic differentiation. *Mineralogical Magazine*, **23**, 317–328.
- Rubatto, D. & Hermann, J., 2003. Zircon formation during fluid circulation in eclogites (Monviso, Western Alps): implications for Zr and Hf budget in subduction zones. *Geochimica et Cosmochimica Acta*, **67**, 2173–2187.
- Salvi, S., Pokrovski, G.S. & Schott, J., 1998. Experimental investigation of aluminum-silica aqueous complexing at 300°C. *Chemical Geology*, **151**, 51–67.
- Selverstone, J., Franz, G., Thomas, S. & Getty, S., 1992. Fluid variability in 2 GPa eclogites as an indicator of fluid behavior during subduction. *Contributions to Mineralogy and Petrology*, **112**, 341–357.
- Sepahi, A.A., Whitney, D.L. & Baharifar, A.A., 2004. Petrogenesis of andalusite-kyanite-sillimanite veins and host rocks, Sanandaj-Sirjan metamorphic belt, Hamadan, Iran. *Journal of Metamorphic Geology*, **22**, 119–134.
- Snelling, N.J., 1957. A contribution to the mineralogy of chloritoid. *Mineralogical Magazine*, **31**, 469–475.
- Snelling, N.J., 1958. Further data on the petrology of the Saxa Vord schists on Unst, Shetland Isles. *Geological Magazine*, **95**, 50–56.
- Sorensen, S.S. & Grossman, J.N., 1989. Enrichment of trace-elements in garnet amphibolites from a paleo-subduction zone: Catalina Schist, Southern-California. *Geochimica et Cosmochimica Acta*, **53**, 3155–3177.
- Tagirov, B. & Schott, J., 2001. Aluminum speciation in crustal fluids revisited. *Geochimica et Cosmochimica Acta*, **65**, 3965–3992.
- Tropper, P. & Manning, C., 2007. The solubility of corundum in H₂O at high pressure and temperature and its implications for Al mobility in the deep crust and upper mantle. *Chemical Geology*, **240**, 54–60.
- Verlagnet, A., Brunet, F., Goffé, B. & Murphy, W.M., 2006. Experimental study and modeling of fluid reaction paths in the quartz-kyanite ± muscovite–water system at 0.7 GPa in the 350–550 °C range: implications for Al selective transfer during metamorphism. *Geochimica et Cosmochimica Acta*, **70**, 1772–1788.
- Walther, J.V., 2001. Experimental determination and analysis of the solubility of corundum in 0.1 and 0.5 m NaCl solutions between 400 and 600 °C from 0.5 to 2.0 kbar. *Geochimica et Cosmochimica Acta*, **65**, 2843–2851.
- Whitney, D.L. & Dilek, Y., 2000. Andalusite-sillimanite-quartz veins as indicators of low-pressure-high-temperature deformation during late-stage unroofing of a metamorphic core complex, Turkey. *Journal of Metamorphic Geology*, **18**, 59–66.
- Whitney, D.L. & Olmsted, J.F., 1998. Rare earth element metasomatism in hydrothermal systems: the Willsboro-Lewis wollastonite ores, New York, USA. *Geochimica et Cosmochimica Acta*, **62**, 2965–2977.
- Widmer, T. & Thompson, A.B., 2001. Local origin of high-pressure vein material in eclogite facies rocks of the Zermatt-Saas zone, Switzerland. *American Journal of Science*, **301**, 627–656.
- Wohlars, A. & Manning, C.E., 2007. Model crustal fluids at high P and T: implications for Al transport. *Geochimica et Cosmochimica Acta*, **71**, A1123.
- Wohlars, A. & Manning, C.E., 2009. Solubility of corundum in aqueous KOH solutions at 700 °C and 1 GPa. *Chemical Geology*, **262**, 310–317.
- Yardley, B.W.D. & Bottrell, S.H., 1992. Silica mobility and fluid movement during metamorphism of the Connemara schists, Ireland. *Journal of Metamorphic Geology*, **10**, 453–464.
- Zeitler, P.K., Barreiro, B., Chamberlain, C.P. & Rumble, D., 1990. Ion-microprobe dating of zircon from quartz-graphite veins at the Bristol, New Hampshire, metamorphic hot spot. *Geology*, **18**, 626–629.

Received 8 June 2009; revision accepted 23 August 2009.